



AirCargoChallenge 2022

Technical Report

Team #14

Lift UP



TABLE OF CONTENTS

1	Introduction	1
2	Project management.....	1
2.1	Organization chart and roles.....	1
2.2	Work and time schedules	2
2.3	Finances	2
2.4	Sponsors and Social Media	3
2.5	Outreach	4
3	Preliminary design	4
4	Aerodynamic design.....	6
4.1	Airfoil design	7
4.2	Wing design.....	10
4.3	Winglet design	12
4.4	Tail design	13
4.5	Fuselage design.....	13
5	Flight Mechanics	15
5.1	Stability analysis.....	15
5.2	Climb Performance	17
5.3	Minimum turn radius.....	17
5.4	Cruise speed estimation.....	18
5.5	Payload prediction	19
6	Structural design	19
6.1	Wing design.....	20
6.2	Fuselage design.....	23
6.3	Cargo bay	24
6.4	Tail design	24
6.5	Landing gear design	26
7	Electronic systems.....	28
8	Outlook	29
9	Drawings	31

1 INTRODUCTION

This report summarizes the design of the small remote-controlled cargo aircraft designed by the Lift UP team, a group of students from the University of Padua (Italy) aiming to compete in the Air Cargo Challenge 2022 in Munich (Germany). The team was founded in 2018 under the supervision of Professor Francesco Picano and has grown over the years to be composed, at present, of over 60 students of the University of Padua coming from various courses of study.

This document encapsulates all the studies and works carried out over the last 3 years from the preliminary design phase through to flight testing of the final aircraft. Strengthened by the experience gained during the previous edition of the competition, which took place in Stuttgart in 2019, we dedicated ourselves to increasing our theoretical and technical knowledge to develop the best aircraft possible. As it will be possible to see inside of the report, we have focused a lot on the optimization of every single subsystem to ensure high performance and limit the weight.

At the end of the design process, our team chose a single high wing aircraft in pusher configuration with an inverted V-tail supported by 2 booms with a tricycle landing gear. The payload is housed within the wide fuselage which is designed to aid in lift generation during flight operations. First, a prototype was built which allowed for validating the developed mathematical tools confirming the goodness of the design. Following a campaign of flight tests, the necessary corrections to the project were made to arrive at the final model presented here that will be the one to participate in this year's competition.

2 PROJECT MANAGEMENT

The project is currently made up of about 60 active members distributed within well-defined working divisions. Each group is organized in such a way in order to assign activities to the various members and periodic updating meetings are then proposed by videoconference or in presence in the university classrooms. During the meetings each division has to update the rest of the team and decide on the continuation of the work. The production activity of the designed aircraft takes place within a laboratory of about 40 m² located within the University facilities.

2.1 ORGANIZATION CHART AND ROLES

Lift UP team is divided in two main branches: the *Technical Branch* that deals with all the technical activities of the project and is supervised by the *Technical Manager*, and the *Administrative Branch* that deals with all the administrative activities useful for the correct functioning of the whole project and is supervised by the *Team Manager*.

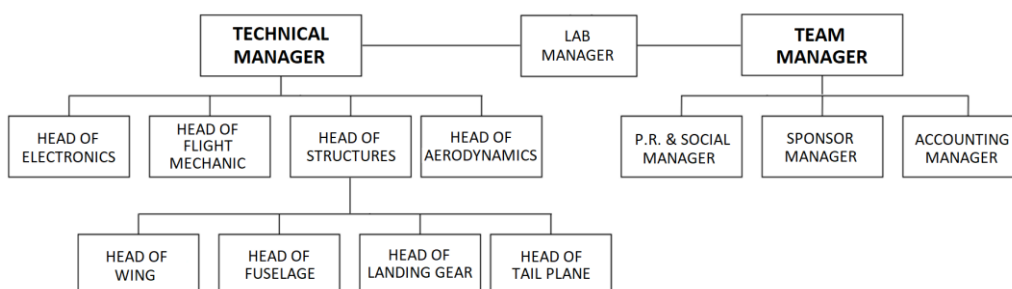


Figure 1 - Organization chart

Within the technical branch, there are the Electronics, Flight mechanics, Structures, and Aerodynamics divisions, each supervised by a manager. In turn, the Structures division has four other figures responsible for the main aircraft subsystems, namely wing, fuselage, undercarriage, and tailplane. In addition to the above figures, there is a third one known as the Laboratory Manager, who is responsible for the activities that are carried out within the laboratory. As such he is required to be aware of the safety risks that may occur in the laboratory itself and to take action to ensure that no hazardous situations occur to the health of workers. The construction of the aircraft is primarily the responsibility of the Structures Division because it knows better than any other branch the process of manufacturing the various components needed. However, any member of the project may contribute to the construction if it is under the supervision of members of the Structures division.

2.2 WORK AND TIME SCHEDULES

Given the short amount of time that typically intervenes from the date of release of the regulation to the competition, it is of critical importance to organize the timing and resources available according to the deadlines in the regulation. The period from October 2019 until the release of the new regulations (6/8/2020) was used to recruit and train the new team, particular attention was paid to the development of sizing procedures that could be used effectively for the development of future aircraft.



As the regulation was published, it has been decided to develop a prototype which would have allowed identifying any criticalities during construction or flight tests. The production of this prototype took about 17 months, but considerable delays were accumulated due to the closure of the laboratories used for the construction of the aircraft as a result of the pandemic, as well as many of the participants had to return to their residences for lockdown. The first flight of the prototype took place on 26/03/2022, more tests were conducted during the month of April to identify the changes to be made to the final design on time for the deadline for the delivery of the tables and the technical report. The most significant modification was the introduction of two lateral fins near the tailplane to increase the longitudinal stability of the aircraft, as the first flight tests showed poor longitudinal pitch stability. The final aircraft is going to be a structural optimization of the prototype, meaning that we are going to make lighter the structures where they proved to be more rigid and resistant than expected with consequent benefit in carrying a greater payload.

At this point the final design is frozen and the production of the final aircraft is expected to start on 1/05/2022 and will last about 45 days, then there will take place as many flight tests as possible until the competition in order to identify the optimal payload able to optimize the flight score.

2.3 FINANCES

In the last years, the Lift UP project has received funding from both the University of Padova and the Department of Industrial Engineering of the University for a total of about 13 000 € per academic year. These funds were granted through a competitive funding call hosted by the University and the Department of Industrial Engineering where we had to submit a complete description of our main objectives and planned activities for the year. We managed to gain almost all the requested funds on each one of the calls, a brief overview of the received and spent funds for the previous years can be found in *Table 1* and *Table 2*.

Table 1 : 2019/2020 Balance Sheet

Academic Year 2019/2020	
Remaining from previous year	€ 77.22
Received Funds	€ 13,960.00
Spent Funds	€ 9,264.58
Net	€ 4,772.64

Table 2: 2020/2021 Balance Sheet

Academic Year 2020/2021	
Remaining from previous year	€ 4,772.64
Received Funds	€ 12,000.00
Spent Funds	€ 8,912.07
Net	€ 7,860.57

During this last academic year, we became the most funded project in the Department of Industrial Engineering since we received about 9000 € from the University and about 4200 € from the Industrial Engineering Department. Having a remainder of about 7500 € from the last academic year, during which all the activities were slowed down due to the pandemic and our expenses were lower, we had access to an ample budget of about 20000€ that enabled us to improve our workshop instrumentation and the materials used for the construction. The main expenses faced during the year are presented in *Table 3* and they are distributed among the various entries. A forecast of the expenses that will be faced in the coming months in preparation for the competition is also presented in *Table 4*. Being at the end of April and having covered all the main expenses, we still have a decent budget available that we decided to keep for the preparation for the competition, to complete the construction of the final version of the aircraft, and to face any unexpected problems that could arise during the next months. Furthermore, any remaining budget will be used for the start of the activities in the next Academic Year after the competition since our next funding call will be held in November.

Table 3: Financial outgoings as of May 1st, 2022

Financial outgoings as of May 1st, 2022	
Prototype	€ 4,500.00
Competition Aircraft	€ 3,200.00
Workshop and tools	€ 4,100.00
Participation Fee	€ 2,650.00
Merchandising	€ 1,500.00
Total outflow	€ 15.950,00

Table 4: Expected outflows for the next months

Expected outflows for the next months	
Prototype	€ 0.00
Competition Aircraft	€ 1,000.00
Workshop and tools	€ 1,000.00
Participation Fee	€ 0.00
Merchandising	€ 200.00
Travel expenses	€ 500.00
Expected outflow	€ 2,700.00

2.4 SPONSORS AND SOCIAL MEDIA

In these last years, the main sponsors of the Lift UP project have been the Department of Industrial Engineering and the University of Padua itself, as you can see in the chapter dedicated to the financial aspects. The department has granted us, in addition to the funds already mentioned, a working space within the structures of the University where we carry out all the work necessary to produce the aircraft.

The project is also committed to getting in touch with local industrial realities and it was able to get two important sponsorship contracts. The first one concerns the company *Carùs s.r.l.*, an important local company that deals with the production and molding of expanded plastic materials. They guaranteed us a supply of polyurethane foam in different densities and a proprietary material specially developed for use as the core of composite materials. The second sponsorship was completed with *Altair Engineering Software*, which provided us with the access to its suite of FEM and CFD simulation software tools, allowing us to extend our knowledge and skills in these areas. We are still working to increase the number of sponsors by continuing to reach out to other local companies that may be interested in working with us.

Our main social channels are our Instagram/Facebook pages, our LinkedIn page and our website (<https://www.teamliftup.it/>) which was created at the end of 2019 as a platform to include all the most important information and contact methods. The website has allowed many of the current team members to get to know, contact and join us. At the moment it is being updated in order to reflect the new additions to our group that has greatly expanded over the past few years. Our Instagram and Facebook pages on the other hand (<https://www.instagram.com/liftup.padova/>) is the main publicity tool for the project and allows us to connect with the University's student community and other student projects. It is the social tool we take care of the most as it is the best way to show through photos, videos, and small stories all of our daily activities, our achievements and the various events we participate in during the year. In recent years we have entrusted the management of the page to a member of the group who, taking care of graphics and content, has allowed a significant increase in the number of followers and reactions. Furthermore for some months we presented on our social media pages a weekly series about curiosities concerning the history of aviation which received much positive feedback. We are also in contact with the University Social Office with whom we are collaborating to create social content shared with the University. The last social channel is the LinkedIn page (<https://www.linkedin.com/company/liftupadova/>) which is mainly used to maintain contact with local companies and to publish sponsored content related to the sponsorships in place, listed in the previous paragraphs.

2.5 OUTREACH

In addition to the publicity work done online through our social pages, the Lift UP project has been engaging in various events, both live and online, intending to publicize the project and propose cultural activities to the population. In particular, we took part in the *European Researchers Night (Veneto Night)* organized by the University during which we presented our project at a local fair together with all the other research projects developed within the University. Another occasion was the *Next Festival*, a two days fair organized by the students' organizations to publicize the projects developed within the Engineering Departments. It was a nice opportunity to share ideas with other projects and to be discovered by many other students who were able to see our prototype. We have also organized numerous presentations both in the classroom, when possible, and online hosted by our reference professor. These are the occasions in which we receive the most attention and they have been the main source of increase in the number of participants that have grown from about 30, at the end of 2019, to the current 60.

At the moment, we have become one of the largest projects in the engineering department and, also thanks to these activities, we have been able to have our Open Badge issued. The Open Badge is an official recognition badge certified by the University that we can issue to the most deserving members of the group to attest the active participation in the project.

3 PRELIMINARY DESIGN

The introduction of a dimensional limit in the regulations that requires the aircraft to be inscribed in a parallelepiped with fixed sides, together with the new scoring methods referred to different aspects of the flight (take-off, climb, maximum altitude reached, cruise), leads to very different design parameters compared to those of previous competitions. Therefore, it was decided to develop an algorithm capable of producing a set of preliminary designs which were then put into competition with each other simulating for each of them the various phases of flight of the aircraft including takeoff, climb, and cruise.

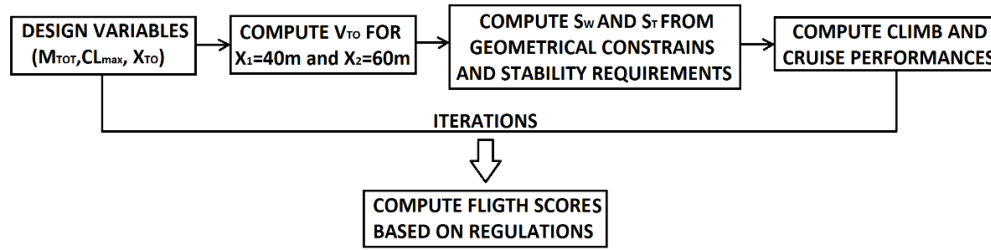


Figure 2 - Flow chart of preliminary design algorithm

The algorithm's input data are:

- *Total mass*: The total mass was split assuming that half of the mass could be attributed to the empty aircraft and the other half to the payload carried. This assumption was made based on the project's prior experience in building aircraft for the ACC.
- *Maximum lift coefficient of the aircraft*: the dual goal of the competition is to carry a heavy payload and cover as much distance as possible in 120 seconds; these goals are conflicting since a great capability of carrying a heavy payload is reached through the use of thick and heavily curved airfoils, and said features entail an elevated drag and thus a slow aircraft. Therefore, the $C_{L,max}$ generated from the airfoil needs to be a compromise between the two mentioned extremes; it was decided that $C_{L,max}$ can vary within the range $1,6 < C_{L,max} < 1,9$ in flapped configuration.
- *Structural Constraints*: Minimum values for wing and tail plane chords were imposed in order to guarantee sufficient structural rigidity and enough room for the installation of servo controls internally to the structures.
- *Performance of propulsion system*: to estimate the performance of the propulsion system the software eCalc has been used considering the AXI Gold 2826/10 motor and APC-E 10x6 E propeller, required by the ACC 2022 regulations. We used a MATLAB code to obtain the power available P_A in function of the airspeed and RPM of the propulsion system.

At this point, the code proceeds as follows:

- 1) Starting from the following simplified equation of the take-off (neglecting ground friction and drag)

$$X_{TO} = M \int_0^{V_{TO}} \frac{V_{\infty}^2}{P_A} dV_{\infty}$$

Where V_{TO} is the takeoff speed and M is the total mass. Two distinct cases with take-off distance respectively of $x_1=40m$ and $x_2=60m$ are analyzed, and the take-off speed for each case is obtained by resolving the previous integral.

- 2) Subsequently, different plausible values of the maximum lift coefficient within the previously defined range are assumed, and for each of them the required wing surface for take-off at the two distances x_1 and x_2 is calculated with the formula:

$$S_w = \frac{2Mg}{\rho V_{TO}^2 C_{L,max}}$$

- 3) After that, a calculation to generate rectangular geometries for the wing and the tailplane was implemented given the dimensional limits set by the regulation; in particular, an approximate longitudinal static stability condition was imposed through the tail volume method. Among the potential solutions, the one with the highest aspect ratio was sought to maximize the efficiency. Once known the wing aspect ratio, it is possible to evaluate the drag coefficient with the formula

$$C_d = C_{d0} + KC_L^2 \quad \text{with} \quad K = \frac{1}{\pi AR_w e}$$

where the drag coefficient at zero lift was presumed to be proportional to the wet surface of wing and tailplane, meanwhile the Oswald efficiency number was calculated with a MATLAB algorithm.

- 4) For every geometry obtained for different values of $C_{L,max}$, total mass, and take-off distance (40m and 60m), the algorithm calculates the performances during the climb phase, in which the power required is considered to be split into power to overcome the drag, and power needed to increase the aircraft altitude ($P_R = P_{drag} + P_{climb}$). Considering the climbing speed constant and neglecting the transition phase, the algorithm calculates optimal speed and optimal ramp angle γ that allows to reach the maximum altitude. A circular trajectory at constant altitude was assumed to evaluate cruise performance, the power required for the turning maneuver is:

$$P_{turn} = \left(AV^3 + \frac{B}{V} \right) \left(\sqrt{1 + \left(\frac{V_{turn}^2}{Rg} \right)^2} \right)^{\frac{3}{2}} \quad \text{with} \quad A = \frac{1}{2} \rho S_w V^2 C_{D,0} \quad , \quad B = \frac{2W^2}{\rho S_w \pi AR_w e}$$

Assuming the power required equal to the power available P_A at max RPM, we can compute the cruise speed by setting the circumference radius equal to the maximum feasible within the airfield perimeter ($R = 120m$), and multiplying it by 120 seconds we obtain the distance travelled.

By executing this algorithm for different values of the input variables, a set of potential solution is obtained; from this set, the configuration that reached the highest score was chosen. So the preliminary design has the following parameters:

Total mass	$M = 6 \text{ kg}$	Cruise speed	$V_{cruise} = 25.2 \text{ m/s}$
Take-off distance	$X_{TO} = 40 \text{ m}$	Take-off speed (at $C_{L,max}$)	$V_{TO} = 11.2 \text{ m/s}$
φ (quadrilateral angle)	$\varphi = 76^\circ$	Cruise coefficient of lift	$C_{L,cruise} = 0.40$
Root wing chord	$c_{root} = 0.20 \text{ m}$	Climb coefficient of lift	$C_{L,climb} = 0.79$
Wing surface	$S_w = 0.425 \text{ m}^2$	Max coefficient of lift	$C_{L,max} = 1.8$

4 AERODYNAMIC DESIGN

As for the aerodynamic design it was decided to adopt a wing with a constant airfoil and a planform composed of a first rectangular central section followed by a tapered external section. To increase the lift generated during take-off, we introduced flaps in the central rectangular section, while the tapered sections will be equipped with ailerons for the roll control of the aircraft. The fuselage has been designed with the intent to satisfy multiple requirements that will be discussed below, from the aerodynamic point of view particular attention has been paid to trying to obtain a fuselage capable of contributing to the formation of lift. The tailplane will have a rectangular shape and a wingspan that will guarantee the largest possible aspect ratio considering the dimensional limits imposed by regulations.

Starting from the lifting surfaces, the main drivers for the aerodynamic design were given by the preliminary design. From these parameters a more detailed design has been developed to optimize the lifting surfaces of the aircraft. Knowing from the new ACC rules the time intervals in which the

drone will be cruising or climbing, we introduce an objective function for the coefficient of drag, defined as follow:

$$f = 0.667C_{D,cruise} + 0.333C_{D,climb}$$

Having some difficulties optimizing both the airfoil and the wing planform together, we chose to optimize at first only the 2D wing airfoil and, subsequently, the whole 3D geometry of the wing considering a constant optimized airfoil along the wing span. The airfoils taken into consideration were the SD7062, used to fly in the previous competition, and two optimized airfoils (opt06v3, opt06v2m). Details about the airfoils are given in the next chapter.

4.1 AIRFOIL DESIGN

To obtain the best possible performance, we thought to create a new airfoil geometry through a process of optimization, whose main objective is to minimize drag (and thus C_D) under climb and cruise conditions. However, optimization of the previous objective function in the absence of constraints causes a tendency to generate very thin airfoils with a low $C_{L,max}$ value, so penalty functions were introduced on the objective function such that the following minimum requirements were met:

- 1) $C_{L,max,flapped} \geq 1.90$ at $Re = 175000$
- 2) $11\% < \text{maximum thickness} < 14\%$

We opted for an inverse design procedure that uses, as decision variables, the control points of the parametrization of C_p distribution along the airfoil, rather than the airfoil geometry itself, since this choice better represents the physical nature of the problem. Another advantage of this approach is that a local change in pressure distribution results in a change to the entire airfoil geometry. This makes convergence of the optimizer easier, because in this way it is unlikely to get stuck in a local minimum and avoids the onset of "noisy" geometries. Below is the flow chart of the algorithm:

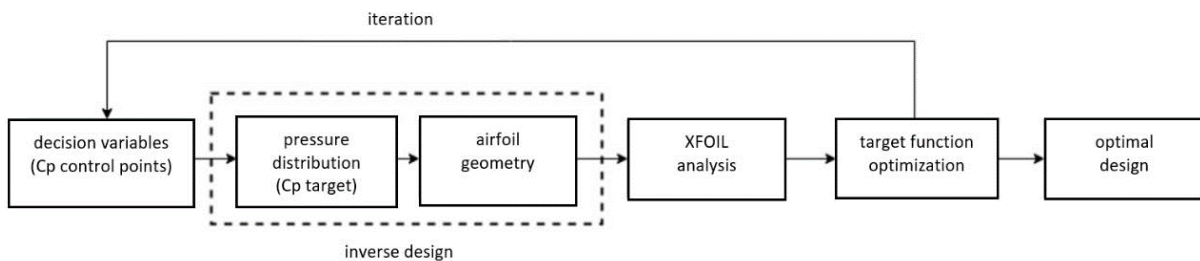


Figure 3 - Flow chart of wing airfoil optimization algorithm

So, the algorithm is developed as follows: for given values of the decision variables a certain CP distribution is obtained, then the DISC approach developed by Dulikravich and Baker¹ along with the Linear Vortex Panel method is used to build the geometric airfoil that produces the C_p distribution determined by the decision variables. The process is iterative: we start with a "zero" geometry of the airfoil, from which we evaluate the differences between its C_p distribution and the target one. Then, the method changes the geometry to try to nullify these differences. This method is relatively accurate while considering angles of attack sufficiently far from the stall condition and is fast to implement and execute.

¹ G. Dulikravich e D. Baker, «Fourier series solution for inverse design of aerodynamic shapes» in International Symposium on Inverse Problems in Engineering Mechanics (ISIP '98), Nagano, 1998.

The generated geometric airfoil is then analyzed in XFOIL obtaining the C_D values at $C_{L,climb}$ and $C_{L,cruise}$, making it possible to evaluate the objective function defined previously. In addition, an analysis is also carried out with the insertion of a flap at 70% of the chord, deflected by 30° , to estimate $C_{L,max}$ in flapped configuration, as to evaluate the penalty function associated with $C_{L,max,flapped}$. The optimization of the objective function was solved with MATLAB's integrated optimization algorithms (genetic algorithm and particle swarm) finally obtaining the optimized opt06v3 and opt06v2m airfoils. The other candidate considered was the SD7062 used in the previous edition of the competition: it has a behavior well known to the team and was chosen mainly for its high efficiency and advantageous shape when considering our fabrication capabilities. Shown below are the airfoils geometries and their C_L vs C_D polars.

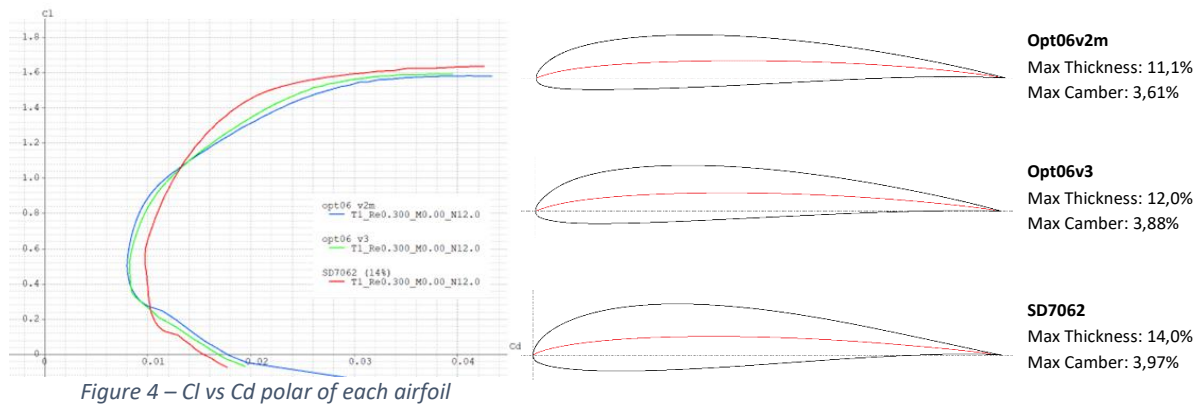


Figure 4 – C_L vs C_D polar of each airfoil

From the polars above we can see that the optimized airfoils generate less drag than the SD7062 over a wide operating range, particularly in cruise and climb conditions ($0.3 < C_L < 1.1$); consequently, their efficiency is higher. All optimized airfoils seem to be stable, giving gentle curves at varying angles of attack and Reynolds number. Comparing the two optimized airfoils we note a very similar behavior, with the difference that Opt06v3 is less efficient for $C_L < 1.1$. However, it should also be noted that Opt06v3 has a higher maximum thickness than opt06v2m which leads to structures with a higher moment of inertia and stiffness. We concluded that the best airfoil for our aircraft is the Opt06v3 because, even if a little less performant than the Opt06v2m, it presents structural advantages.

The optimization conducted, however, can be considered reliable only in operating conditions far from stall due to the inherent limitations of the linear vortex panel method, for this reason, a CFD analysis was conducted for near-stall conditions. The geometry was meshed using a hybrid mesh capable of ensuring adequate resolution of the boundary layer; in addition, the $k\omega - SST$ turbulence model and second order numerical schemes were used for greater accuracy in the solution. We obtained the following results:

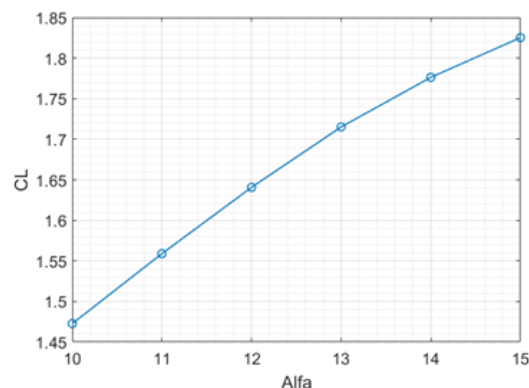


Figure 5 - C_L vs α

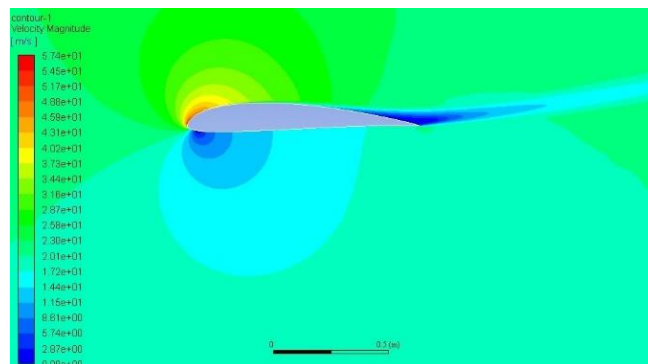


Figure 6 – Velocity magnitude at $\alpha = 15^\circ$

We can see that the airfoil shows a smooth approach to stall and the $C_{L,max}$ obtained is higher than 1.83, so it is more optimistic than the results of XFLR5 and this suggest the flapped configuration satisfies the target values. In *Figure 6* we can see the velocity magnitude around the airfoil at $\alpha=15^\circ$ and the behavior seems to be stable with a detachment of the flow near the 60% of the chord. Finally, a study has been conducted to quantify the performance degradation of the airfoil in the presence of geometric errors that may arise in the production phase of the airfoil itself. For this purpose a MATLAB code has been developed as follows:

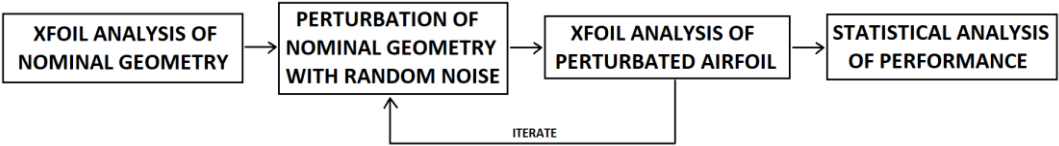


Figure 7 - Flow chart of sensibility analysis algorithm

The nominal geometry of the airfoil is analyzed in XFOIL, then a set of geometries perturbed by Perlin noise are produced from it. This type of noise is characterized by "coherent" random perturbations, i.e., neighboring points have neighboring values, while still maintaining randomness. Each produced geometry is analyzed in XFOIL to obtain their polars, the analysis was conducted at $Re = 300k$ and $N_{crit} = 9$. When the data set is large enough we proceed with a statistical analysis of the results, this study was conducted for different values of the perturbation amplitude. In the case of amplitude equal to 0.2% of the chord (corresponding to a geometric tolerance of 0,5mm) the following results are obtained:

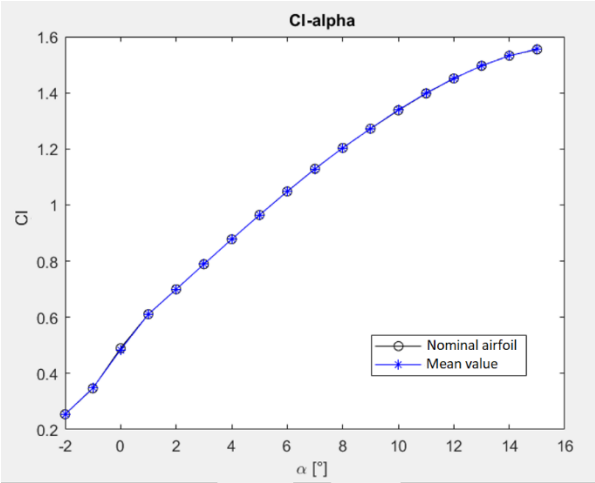


Figure 8 - Cl vs alpha

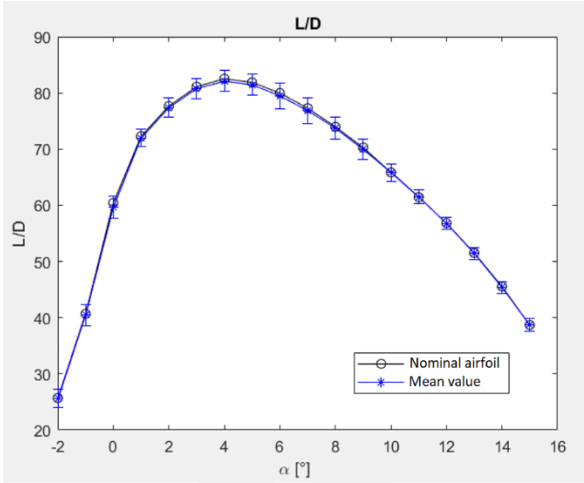


Figure 9 - Airfoil efficiency vs alpha

EFFICIENCY UNCERTAINTY (Noise Amplitude @ 0.2% of the chord)			
Angle of attack	0°	5°	10°
Nominal efficiency	60.43	81.87	65.85
Mean perturbed efficiency	59.71	81.44	65.82
Relative uncertainty	3.25%	2.35%	2.44%

The opt06v3 airfoil proves to be robust, especially in the generation of lift; in fact, only minimal variations in the C_L curve are noted with respect to the nominal geometry. The performance perturbation, although small, is mainly related to C_D , which explains the drop in efficiency of a few percentage points of the perturbed airfoils; however, the values obtained are more than satisfactory. It can be concluded that by guaranteeing a geometric tolerance in the construction phase within 0.5 mm (value in line with our production capacity) the performance obtained is line with the nominal geometry.

Studies conducted in the past within the project suggest that the optimal flap positioning is around 70% of the chord with a maximum deflection not higher than 30°. By adopting these values we obtained an increase of $C_{L,max}$ equal to 0.3 from XFLR5 analysis, bringing the $C_{L,max}$ developed by the airfoil to 1.9 and, therefore, in line with the project requirements; however it must be underlined that the results supplied by this software cannot be considered completely reliable at high angles of attack.

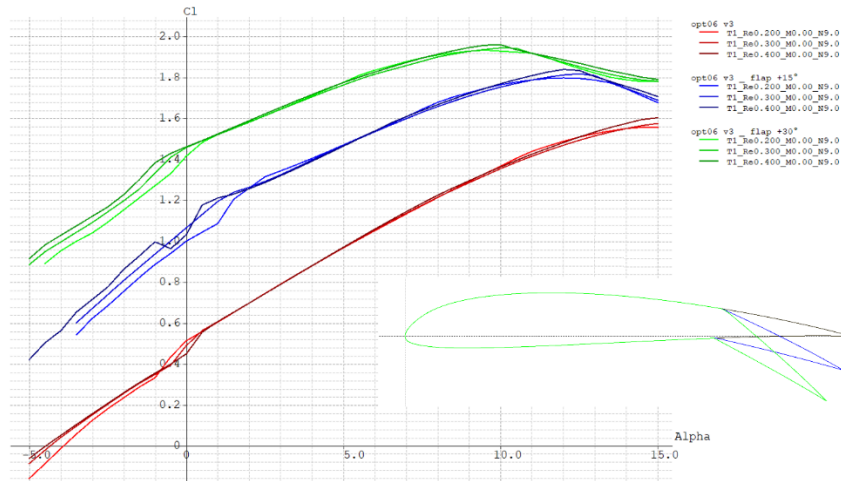


Figure 10 - C_l vs alpha at different flap deflections and Reynolds Number

In any case, from the polars obtained it is possible to note the high regularity of the curves as the Reynolds Number varies, so a stable behavior of the airfoil is expected at different operating ranges.

4.2 WING DESIGN

The wing geometry was also the result of numerical optimization, considering the reduced aspect ratio caused by the dimensional limits set by the regulation, it was decided to adopt a tapered wing to reduce the induced drag. This geometry also allows to have a more efficient distribution of masses than a rectangular or elliptical wing. In particular, we choose to have a rectangular-plan central part (for construction simplicity) followed by a single taper applied on the trailing edge of the airfoil to help the positioning of the wing spar during structural design. The decision variables of the optimization problem are therefore 5: root chord, tip chord, the position of tapering, middle section twist and tip twist (shown in the figure below). Since the wing is tapered, it is necessary to apply a twist to the airfoils to obtain an adequate stall behavior; therefore the code has been realized to try to guarantee a minimum stall distance for each airfoil span at the Reynolds at which it operates (Reynolds varies because the wing is tapered).

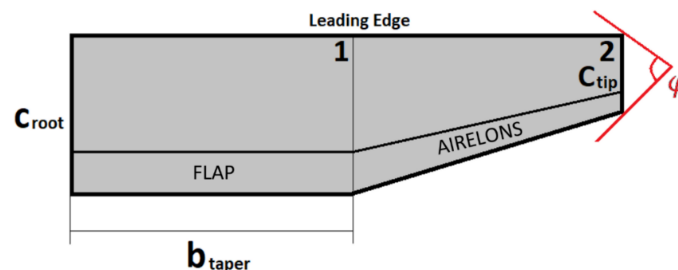


Figure 11 - Wing planform's main geometry properties

The following design constraints are assumed:

- $\varphi = 38^\circ$ from the preliminary design (angle of the quadrilateral in which the aircraft must be inscribed): for fixed values of chord and b_{taper} , φ determines the length of the wing;
- $C_{L,max,flapped} \geq 1.8$;
- $Twist\ angle \leq -2^\circ$;

The optimization was conducted using constant airfoil Opt06v3 along the wing. The optimization has been implemented in MATLAB using a genetic algorithm and particle swarm to minimize the objective function already introduced in the previous pages. So, the optimization algorithm controls the generation of decision variables individuals, then OpenVSP software takes care of generating the geometry and then analyzes it using the Vortex Lattice Method. Now we obtained the C_D in climb and cruise conditions and we can evaluate the objective function defined above.

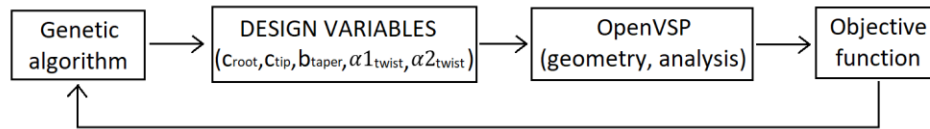


Figure 12 - Flow chart of wing's optimization algorithm

As a result of the optimization, a wing having the following geometric data is obtained:

Optimal values for decision variables		Optimal values for wing geometry	
Root chord	$c_{root} = 0.269 \text{ m}$	Wing span	$b = 2.15 \text{ m}$
Tip chord	$c_{tip} = 0.132 \text{ m}$	Wing surface	$S = 0.512 \text{ m}^2$
First segment length	$b_{taper} = 0.466 \text{ m}$	Aspect Ratio	$AR = 9.03$
Middle section twist	$\alpha_{1,twist} = -0.2^\circ$	Mean aerodynamic chord	$MAC = 0.246 \text{ m}$
Tip twist	$\alpha_{2,twist} = -1.5^\circ$	Taper ratio	$\lambda = 0.49$

The wing planform and lift distribution generated by the wing under cruise conditions obtained with XFLR5 is shown Figure 13: the distribution of lift (in red) is regular and there are no abnormal peaks, also if compared with the elliptical distribution of lift (in gray) is noted an excellent similarity between the two curves which grants particularly high Oswald factors, confirming the goodness of the design.

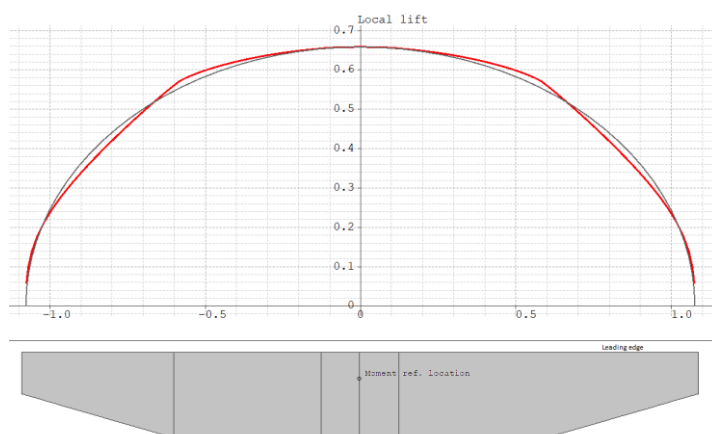


Figure 13 - Wing's lift distribution compared with the ideal one

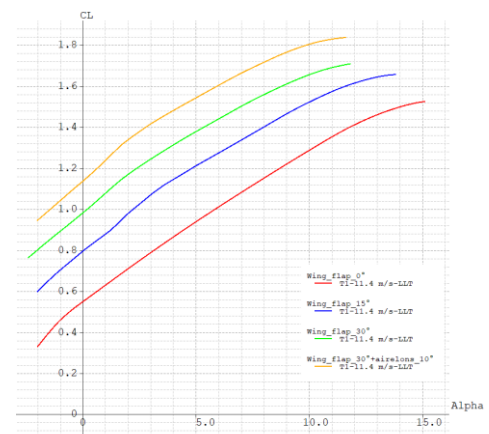


Figure 14 - Wing C_L - α at different flap deflections

To conclude, the polars of the wing with and without deflected flaps obtained with Lifting Line Theory are presented in Figure 14. With the flaps deflected to 30° a $C_{L,max}$ of 1.7 is obtained (green curve), i.e. 0.1 less than the requirement value. Consequently, it was decided to impose a downward deflection of 15° also on the ailerons to make them work as flaps, in this way the wing show a $C_{L,max}$ near 1.8 (yellow curve), in line with the design constraints.

4.3 WINGLET DESIGN

It is well known that induced drag is high at high AoA, a condition that occurs especially during takeoff, climb and landing. Reducing the induced drag is particularly useful to minimize the takeoff run and maximize the subsequent climb rate, which are both important aspects to maximize the flight score. To decrease the induced drag we decided to introduce winglets, which are particularly effective in our case considering the low aspect ratio of the wing. Consequently, a literature search was conducted on the optimal geometric characteristics to obtain high performance winglets and, after a series of iterations, it was decided to adopt the following geometric characteristics:

Tip airfoil:	PSU 90-125
Cant angle	5°
Sweep angle:	30°
Taper ratio:	0.5

A CFD analysis was then carried out using ANSYS Fluent in order to verify the effective decrease in induced drag produced by the use of winglets. This analysis was carried out at $V = 14\text{m/s}$ and $\alpha=7.3^\circ$ (operating condition, intermediate between take-off and climb). The geometry was meshed using a hybrid mesh, we used Kw-SST turbulence model and second order numerical schemes. The following results were obtained:

	C_L	C_D	E
Wing (XFLR5)	0.992	0.03999	24.81
Wing (CFD)	0.840	0.04922	17.07
Wing + winglet (CFD)	0.875	0.04924	17.77

Comparing the results without winglets obtained in XFLR5 and CFD, there is a discrepancy of 20% in C_L and C_D prediction, due in part to the limitations of the Vortex Lattice Method used in XFLR5 which provides accurate results only at low AoA. Comparing the CFD results with winglet we can see an apparent non-variation of the C_D : this happens because for the way the simulation has been done, the benefit of the winglets is found in an increase of the C_L (+4,17%). To appreciate the decrease of induced drag it would be necessary to compare the results with the same C_L . In conclusion, the use of winglets leads to an increase of 4.10% in efficiency at the speed and AoA considered, this confirms the goodness of the design.

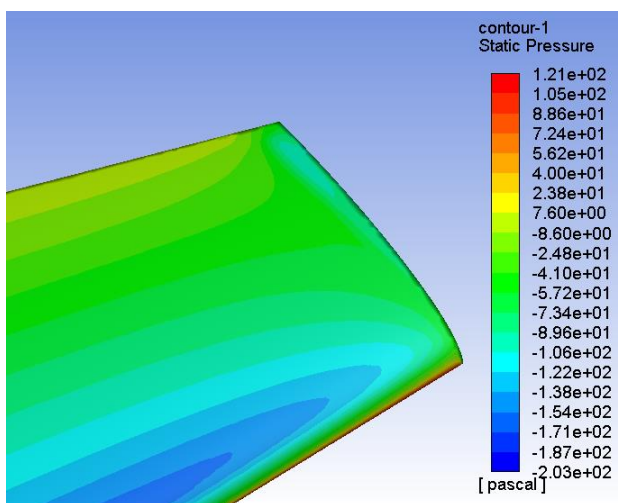


Figure 15 – Static relative pressure without winglet

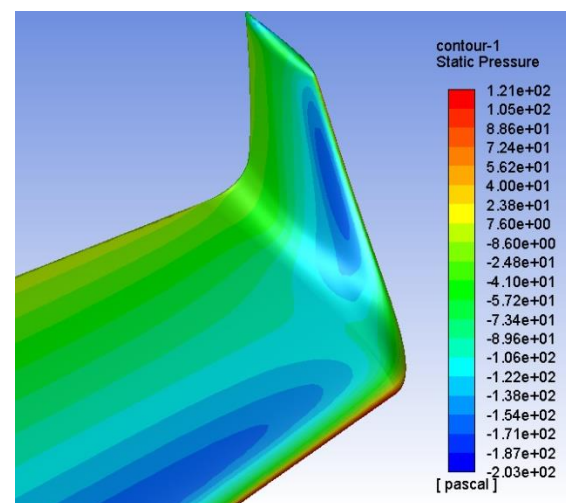


Figure 16 - Static relative pressure with winglet

A further confirmation of the quality of the design can be seen by observing the static pressure field on the suction side of the wing. At the tip, the presence of the winglets attenuates the increase of static pressure induced by the tip vortices and therefore contributes to increase the produced C_L .

4.4 TAIL DESIGN

Firstly, we selected a few airfoils for the tail with the following characteristics:

- maximum thickness equal or greater than 8% of the chord length (due to the structural reason and manufacturing process);
- high efficiency at low angles of attack, wide range of operativity without stall.
- symmetric (no camber);

Our reference was the HT14 airfoil which was successfully adopted in the previous competition. In fact, the need for a new airfoil was determined by the change of the manufacturing process, for which the HT14 doesn't satisfy the maximum thickness driver (being it 7.5% of the chord's length). Instead, the Joukowski 0009 has a maximum thickness of 9% at 25% of the chord. Below are shown the two airfoils and their polars in their Reynolds Number operative range.

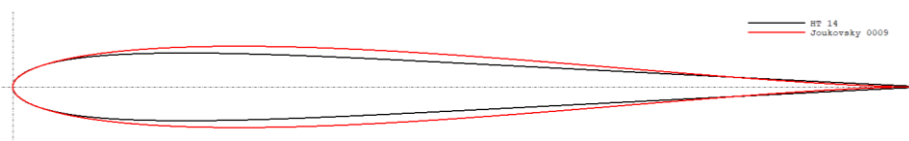


Figure 17 - Tail's airfoils shape comparison

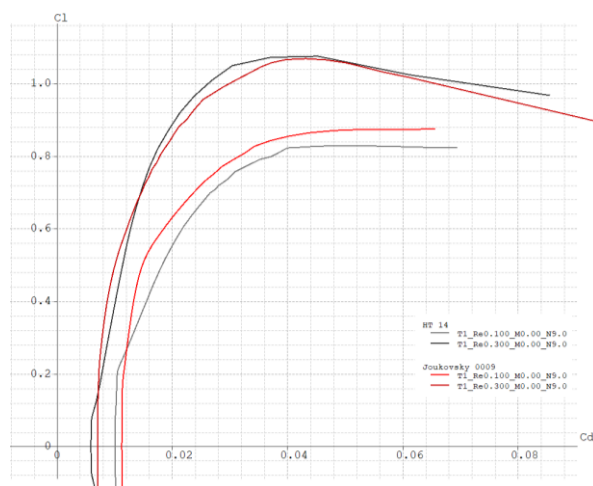


Figure 18 - Tail's airfoils C_l vs C_d comparison at $Re=1e5$ and $Re=3e5$

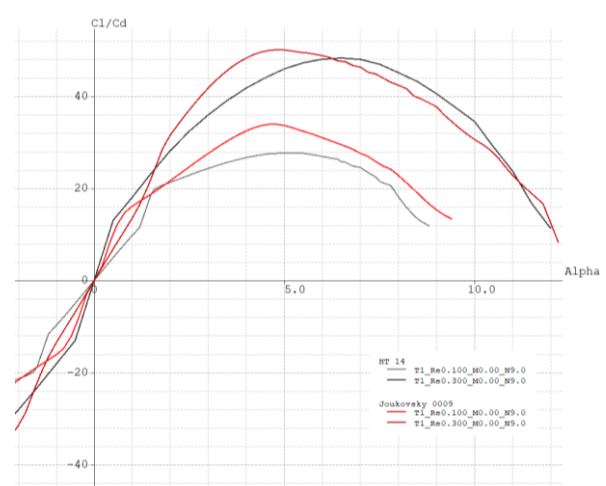


Figure 19 - Tail's airfoils efficiency vs alpha comparison at $Re=1e5$ and $Re=3e5$

We chose to opt for the Joukowski 0009 airfoil because of its similarity with the HT14 airfoil and its higher efficiency for angles greater than 1.5° . The only drawbacks, compared with its predecessor, are a slightly higher drag coefficient near zero degrees angle of attack, however, this behaviour derives from the fact that the Joukowski 0009 is thicker than the HT14.

The shape of the plan is rectangular for reasons related to an easier interfacing with the remaining subsystems of the aircraft, while the value of the chord and the surface has been determined with the dimensioning described in the chapter on flight mechanics.

4.5 FUSELAGE DESIGN

We decided to build a fuselage capable of containing the payload, therefore its geometry must be wide enough to contain the blood bags, but given the low density of the water, the volume of all the bags is substantial, thus leading to a voluminous fuselage. We can try to take advantage of the big volume of the fuselage by involving it in the generation of lift. However, the big frontal area suggests us to not use a pull-propeller configuration because in this case the fast flow produced by the propeller will flow around the fuselage and causes a lot of drag, so we came up with a pusher configuration for the propeller. To avoid the turbulent flow of the propeller on the tail surfaces, the tail has an inverted V geometry connected to the booms. So in the aerodynamic design of the fuselage we considered the following design drivers:

- cargobay position and dimensions;
- center of mass position;
- needed space to put in the wings' longerons and other elements to place inside it.
- maximizing the airflow reaching the pusher propeller;
- position of the landing gears;

The position of the cargobay has been chosen to be as close as possible to the center of gravity of the aircraft, in such a way to minimize the disturbance torques around the three axes of the aircraft that may arise as a result of the sloshing caused by the blood bags inside the cargobay. The pushing propeller configuration tends to bring the center of gravity towards the back of the aircraft, therefore to keep the center of gravity in the correct position it was decided to act on the battery positioning. At this stage, it is important to have the most accurate estimate of the masses of the various subsystems, to design a fuselage that can guarantee a sufficiently forward positioning of the battery.

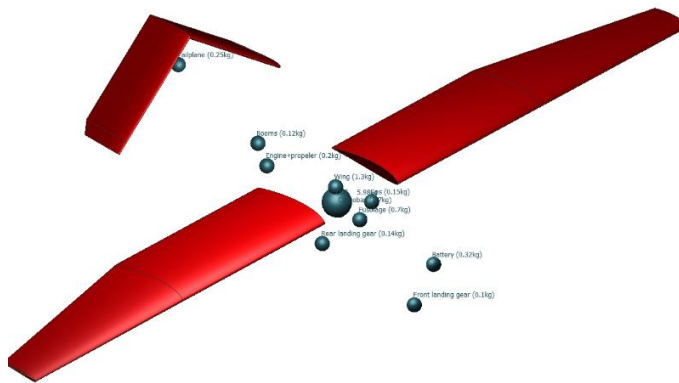


Figure 20 - Position of most important masses

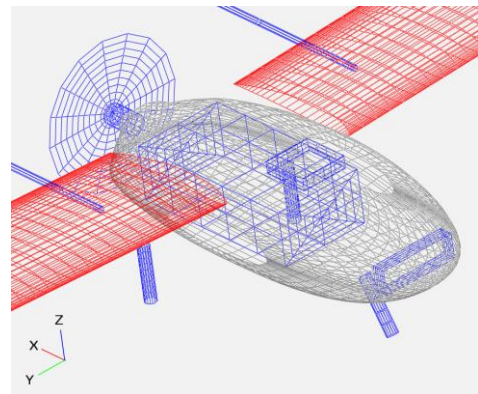


Figure 21 - Position of elements inside the fuselage

We kept a flat portion on the rear to serve as the motor interface, consequently, flow will certainly separate in this area; however we expect the propeller frontal low-pressure zone contribute to reduce the effects of separation. To guarantee some lift generation, we shaped the sections to be similar enough to an airfoil giving a certain mean line curvature. By analyzing the fuselage alone with OpenVSP using VLM method, we obtained after various manual design iterations a small lift coefficient (Figure 22) about $C_L = 0,085$ for $\alpha = 0^\circ$ to a max of $C_L = 0,23$ for $\alpha = 10^\circ$. As a validation, we proceeded with a CFD analysis in Fluent ANSYS under cruising conditions, in particular a hybrid mesh was used with Kw-SST as turbulence model and second order numerical schemes.

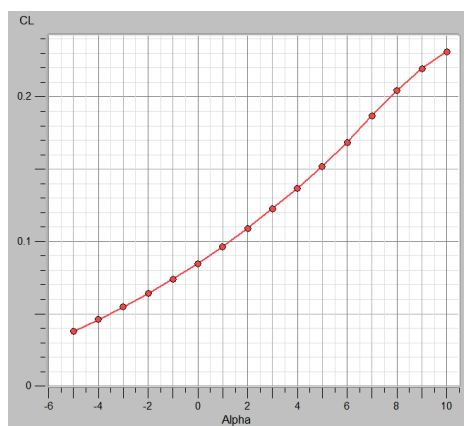


Figure 22 - Fuselage C_L vs α

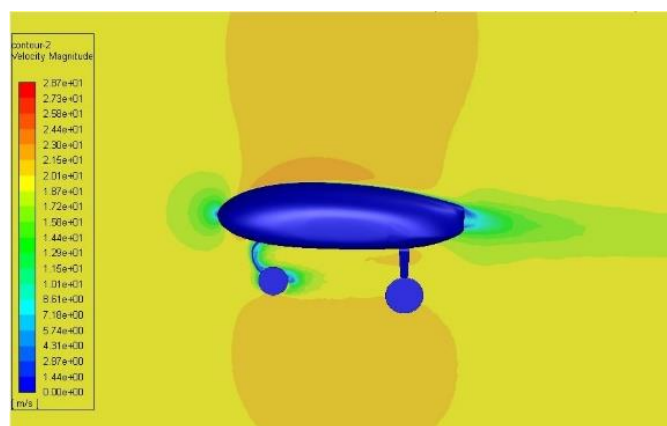


Figure 23 - Mid-plane velocity magnitude at $\alpha = 0^\circ$

From the velocity magnitude graph obtained by CFD, it can be observed that the flow tends to recirculate in the area behind the fuselage as we expected, however, having properly shaped the rear surface of the fuselage, we note that this recirculation area appears very limited and does not

develop a particularly intense wake. Moreover, we notice a stagnation area downstream of the front undercarriage, which has led to a redesign the front carriage in order to reduce the aerodynamic impact.

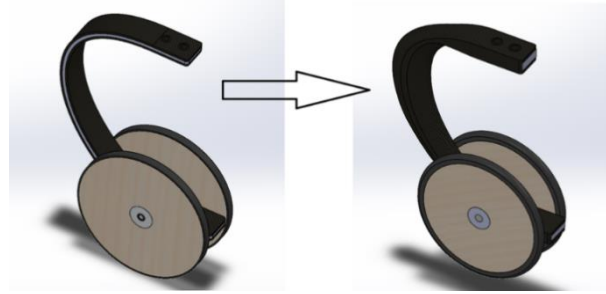


Figure 24 - Evolution of the front undercarriage design

5 FLIGHT MECHANICS

Starting from the detailed design of the wing it was possible to size with greater accuracy the tailplane and the wing dihedral in such a way to ensure sufficient stability and controllability of the aircraft; in addition, the main flight performances have been analyzed to verify that they meet the requirements defined in the preliminary phase.

5.1 STABILITY ANALYSIS

In order to ensure the stability of the aircraft, it is necessary to ensure that the derivative of the moment coefficients relating to rotations along the 3 main axes (pitch, roll and yaw) have an appropriate value. The following target values have been established from values of previously built and tested airplanes, with stability characteristics deemed appropriate by the pilot.

$C_{m,\alpha}$ (pitch)	$C_{n,\beta}$ (yaw)	$C_{l,\beta}$ (roll)
$1.095 \cdot 10^{-2}$ ($SM = 10.2\%$)	$8.094 \cdot 10^{-4}$	$4.178 \cdot 10^{-4}$

For the pitch and yaw axes this condition was obtained by sizing the tailplane and checking the centre of mass position. We use the following equations derived from Paul E. Purser and John P. Campbell² for the "V" tailplane:

$$S_T = \frac{S_w C_{m,\alpha_T}}{\frac{l_t}{C_w} C_{L,\alpha_T} \left(1 - \frac{\partial \varepsilon}{\partial \alpha}\right) \cos^2 \Gamma} \quad S_T = \frac{S_w C_{n,\beta_T}}{\frac{l_t}{b_w} K C_{L,\alpha_T} \left(1 - \frac{\partial \sigma}{\partial \beta}\right) \sin^2 \Gamma}$$

These two make it possible to correlate the various geometrical characteristics (tail surface S_T , wing chord C_w , wing surface S_w , tail arm l_t , tail dihedral angle Γ , aspect ratio AR) with the derivatives of the stability coefficients for the tail, namely C_{m,α_T} and C_{n,β_T} . The K parameter and the derivatives of the parameters of downwash $\partial \varepsilon / \partial \alpha$ and sidewash $\partial \sigma / \partial \beta$ have been estimated by means of empirical formulas, that are function of the geometrical parameters. Initially these equations were applied to previous models built by the Lift UP Team in order to verify their accuracy compared to the models developed in XFLR5. An error on the surface obtained was found not to exceed 5%, demonstrating the applicability of the above equations. Since many unknown geometric parameters of the tail are required in input, the equations have been solved iteratively for different values of tail arm and tail dihedral angle. Among the various solutions obtained we excluded those that exceeded

² Campbell, J. P. Experimental verification of a simplified vee-tail theory and analysis of available data on complete models with vee tails (No. NACA-WR-L-212), 1945.

the geometric limits of the quadrilateral. After some iterations, the final parameters identified for the tailplane are the following:

Tailplane chord	LE wing – LE tailplane	Semi - span	Dihedral angle	Total surface area
0.16 m	0.645 m	0.345 m	-40°	0.11 m ²

To ensure the chosen $C_{m,\alpha}$ is reached, it must be verified that the distance between the neutral point of the complete airplane and its center of gravity is equal to that given by the relation $C_{m,\alpha} = a/MAC(x_N - x_{CG})$. Knowing the wing and tailplane geometry, we obtained $x_N = 0.107$ m (defined by the wing leading edge toward the aircraft tail), so the only unknown in the previous relation is the coordinate of the center of mass of the aircraft, which is equal to $x_{CG} = 0.082$ m. This value was guaranteed during the fuselage design phase by the positioning of the battery, as already described in Chapter 4.4. If the payload transported will vary from the predicted value, we will ensure the required static margin by using a heavier/lighter battery or by adding a ballast into the fuselage.

The stability along the rolling axis was then analyzed and the dihedral of the wing was adjusted to provide adequate behavior. The target values of stability has been reached by an iterative process comparing different configurations of dihedral through Xflr5, the final values are:

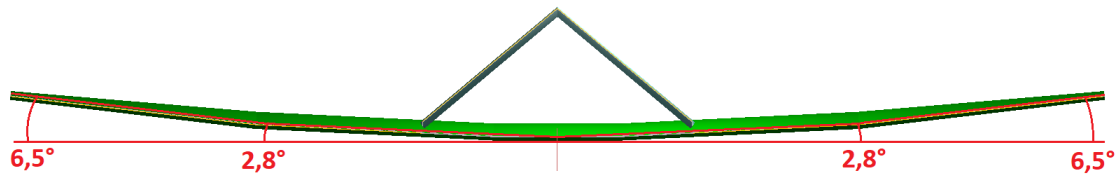


Figure 25 – Dihedral of the wing

It is noted that the dihedral is particularly high, which is due to the fact that the tailplane in an inverted V-configuration which contributes with a negative dihedral effect on roll stability, consequently, to compensate for this effect it is necessary to act more on the dihedral of the main wing.

Following the construction and flight test of the prototype, we observed a reduced stability along the pitch axis, this adversely affected the piloting of the aircraft making it "nervous" and also preventing the attainment of the maximum achievable throttle. It was therefore decided to add two horizontal fins near the tailplane in order to move towards the neutral point of the aircraft. The choice to add such fins and not to intervene on the resizing of the movable surface is due to the need to maintain the nominal geometry of the tail surfaces fixed because, in the case of flight accident in proximity to the competition, it's possible to use the already constructed tailplane as a replacement component. As a result of the addition of these fins, the following final stability values are obtained:

$C_{m,\alpha}$ (pitch)	$C_{n,\beta}$ (yaw)	$C_{l,\beta}$ (roll)
$1,483 \cdot 10^{-2}$ ($SM = 13\%$)	$8.355 \cdot 10^{-4}$	$4.607 \cdot 10^{-4}$
Neutral Point	Center of Mass	Tail Volume
$x_N = 0.114$ m	$x_{CG} = 0.082$ m	0.49

Trimming of the aircraft pitch is done by handling the entire V-tail surface, we decided to adopt a completely movable surface for two main reasons:

- This solution doesn't create a surface discontinuity that affects the aerodynamic performance of the tail due to the clearance between the fixed surface and the control surface
- With this solution we can easily change the tilt angle of the tail and thus reduce the risk of an incorrect alignment of the tail surface due to the construction tolerances

Then, the trimmability to the pitch of the aircraft in cruise and in the condition of takeoff with extended flaps has been verified, thus obtaining the following results:

Tailplane AoA of trim in cruise condition	Tailplane AoA of trim in takeoff condition
$\alpha_{trim,cruise} = -2.1^\circ$	$\alpha_{trim,takeoff} = -3.5^\circ$

These values are well within the operating range of the airfoil ($-8^\circ < \text{AoA} < 8^\circ$ at $\text{Re}=100\text{k}$) and therefore the trim of the aircraft is guaranteed. Finally, we report the graph of the coefficient of pitch moment in trim conditions in cruise and take-off (with extended flaps) conditions obtained in XFLR5, while in *Figure 27* the panel distribution of the XFLR5 analysis is reported.

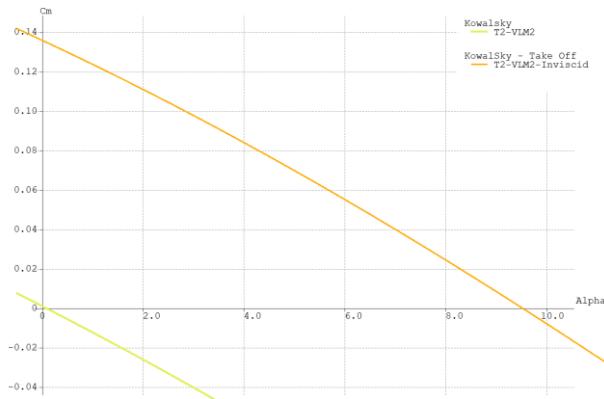


Figure 26 – C_M vs α trimmed in cruise and take-off conditions

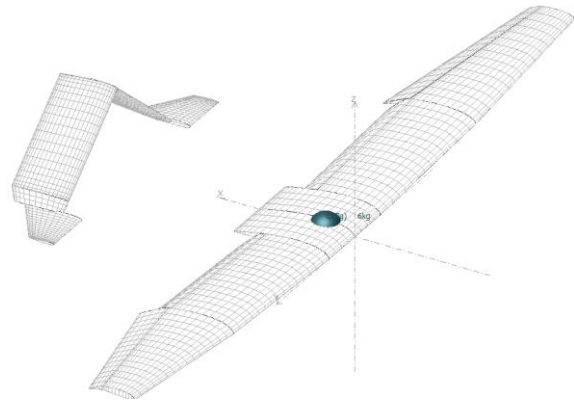


Figure 27 – Panel distribution analyzed in XFLR5

5.2 CLIMB PERFORMANCE

In this analysis we paid our attention to the transition and to the climb stage, with the aim of obtaining the rapid climb speed and the height reached by our aircraft. The assumption we made to study the transition (intermediate phase between takeoff phase and climb phase) is that the aircraft follows approximately a circular trajectory. Besides, we supposed that the lift coefficient related to the transition is equal to the 90% of the maximum lift coefficient. Knowing the power available P_A and the power required P_R , the rapid climb speed is computable through the following expression:

$$\frac{\partial P_A}{\partial V} = \frac{\partial P_R}{\partial V}$$

Successively, considering the previous formula and the assumptions we made, it is possible to evaluate the main parameters necessary for the computation of the final height reached. Observing the results, it can be noted that the values concerning the transition are reasonably negligible. Finally, it is noted that we obtained a value of the reached final height consistent with our target.

V_{climb}	$V_{vertical}$	Δh_{trans}	Δt_{trans}	Δt_{climb}	Δh_{climb}
17.3 m/s	1.1 m/s	0.05 m	0.037 s	60 s	53.7 m

5.3 MINIMUM TURN RADIUS

It is useful to compute the minimum turn radius to understand the maneuverability limits of the designed aircraft. The parameters limiting the minimum turning radius are: the maximum load factor $n_{z,max}$, the maximum lift coefficient $C_{L,max}$ and the available power P_A . The minimum turning radius (for a sustained and correct turn) as a function of speed, expressed in relation to the previously mentioned parameters, is expressed as:

$n_{z,max}$ Limit:	$C_{L,max}$ Limit:	$P_{A,max}$ Limit:
$R_{min} = \frac{V^2}{g\sqrt{n_{z,max}^2 - 1}}$	$R_{min} = \frac{V^2}{g\sqrt{\left(\frac{\rho S C_{L,max}}{2Mg}\right)^2 V^4 - 1}}$	$R_{min} = \frac{V^2}{g\sqrt{\left(\frac{E_{max}}{MgV}\right)^2 P_A^2 - 1}}$

Assuming $n_{z,max} = 2.5$ (corresponding to the static test of lifting the aircraft from its wing ends, considered to be the most critical load condition), the following curves can be plotted as a function of V:

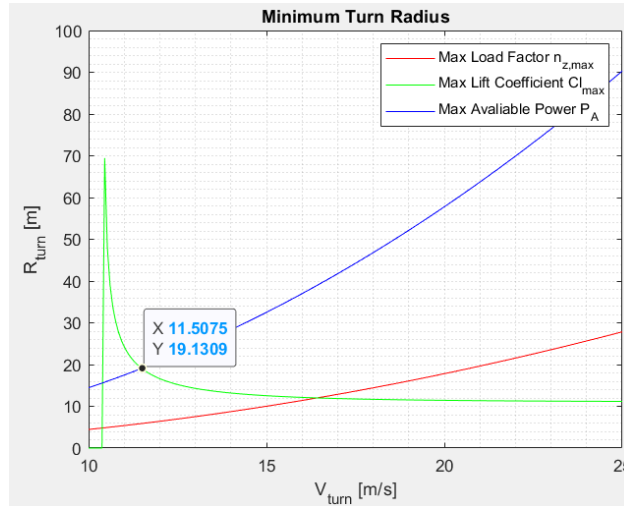


Figure 28 - Minimum turn radius

Noting that the factors that limit the minimum turning radius are the maximum C_L and the available power P_A , from the intersection of the two curves we obtain the following results

$R_{min} = 19,13m$	$V_{Rmin} = 11,5m/s$	$n_{ZRmin} = 1,22$
--------------------	----------------------	--------------------

5.4 CRUISE SPEED ESTIMATION

We estimated the power required by the aircraft in equilibrium condition (lift = weight, drag = thrust) in function of the airspeed with the following expression

$$P_R = AV^3 + BV^{-1} \quad \text{with} \quad A = \frac{1}{2}\rho S V^2 C_{D,0} \quad \text{and} \quad B = \frac{2W^2}{\rho S \pi A Re}$$

Then from the engine + propeller performance we calculated the power available as a function of the airspeed and RPM and we obtain the following graph:

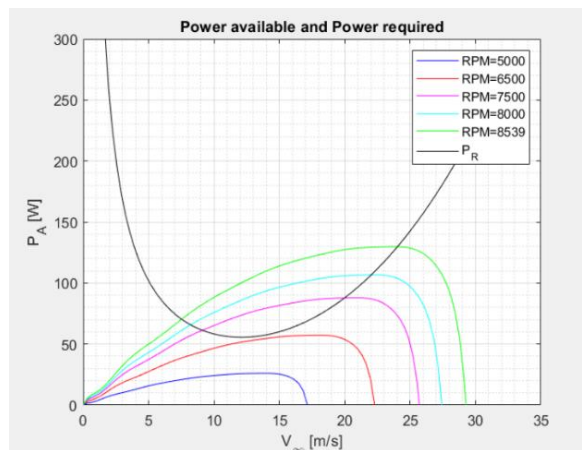


Figure 29 - Power available and Power required in function of V and RPM

We can see that below a minimum value of the motor throttle (6500 RPM) the aircraft cannot fly in equilibrium conditions, and we can see that for any particular value of the motor throttle above 6500RPM there are two possible flight speeds. We only considered the rightmost solution because of propulsive stability. In the end we can see that the maximum theoretical flight speed is about 24,03 m/s and we used this value to size servo controllers in the worst-case scenario (considering that $C_{D,0}$ was underestimated due to the absence of the fuselage, landing gear, etc, and for this reason the real maximum flight speed would be considerably lower).

5.5 PAYLOAD PREDICTION

To compute the expected carried payload in relation to the air density, we examined which phase of the flight has the greatest influence on this parameter. It was observed that the most critical phase is the take-off, since even a moderate decrease in air density would cause the target takeoff distance to be exceeded. A modelling of the take-off phase was conducted through MATLAB script, taking into consideration several parameters (power of the engine, aircraft aerodynamics, rolling friction, ground effect), to verify the maximum payload to carry ensuring to take off in 40m. Still using MATLAB, a linear interpolation to least squares of the obtained data was carried out, extracting the following relation:

$$M_{payload} = 1.962\rho - 0.407$$

With $\rho[kg/m^3]$

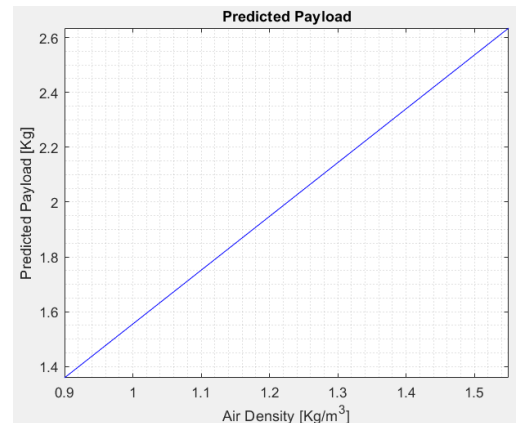


Figure 30 - Predicted payload

6 STRUCTURAL DESIGN

In this phase, the structures have been designed in such a way as to be able to support the maximum loads foreseen on the ground during the required load tests and in flight. Due to the nature of the competition, which requires the development of an aircraft with a high payload to empty weight ratio, it is essential to develop efficient structures with not too high safety margins. However, the structural design of the aircraft is strongly linked to its production, therefore at this stage, it is necessary to keep in mind some limitations due to:

- manual capabilities;
- tools available;
- limitations of the building method.

In order to meet these requirements it was decided to make extensive use of composite materials, such as carbon fiber and Kevlar in epoxy matrix, and sandwich panels. These production techniques ensure the realization of particularly efficient structures and guarantee a production process easily replicable and sufficiently independent of the operator's skills (unlike processes used in the past such as the assembly of wooden structures). In this regard, we have been able to make use of the experience gained in the past on the lamination of composite materials. In the following chapters, the design of the aircraft subsystems will be discussed in detail.

$$K_{f,Kow} = \frac{48EI}{L^3} \quad \text{Eq. 5.1.1}$$

where E stands for elasticity modulus and I stands for inertia momentum of the rectangular hollow section of equation $I = [BH^3 - (B - 2s_{in})(H - 2s_{in})^3]/12$. As the thickness s_{in} varies, the number N of plies making up the laminate also varies. To each ply it is possible to associate a generalized stiffness matrix³. At this stage is possible to compute the laminate engineering parameters⁴

$$E_x = \frac{1}{a_{11}^*}, \quad E_y = \frac{1}{a_{22}^*}, \quad G_{xy} = \frac{1}{a_{66}^*} \quad \text{Eq. 5.1.2}$$

As the thickness s_{in} varies, the axial stresses in the laminate also varies. The maximum bending σ_{max} and torsion τ_{max} stresses can be calculated with

$$\sigma_{max} = \frac{M_f}{W_f}, \quad \tau_{max} = \frac{M_T}{2As_{in}} \quad \text{Eq. 5.1.3}$$

where $W_f = [BH^3 - (B - 2s_{in})(H - 2s_{in})^3]/(6H)$ and $M_T = 20 Nm$ due to the tailplane.

To establish a limit stress criterion we used the buckling theory. Thanks to the global buckling theory⁵, in the case of a beam with fixed constrain at one end and free at the other with axial load, we can determine the critical spar stress inside the section using Euler's equation

$$\sigma_{crit,E} = \frac{EI}{A} \left(\frac{\pi}{kL_1} \right)^2 \quad \text{Eq. 5.1.4}$$

where $L_1=1075$ mm stands for the semi-spar length, k is a parameter that depends on the beam's constraints ($k=2$ for this condition), A stands for spar's section and EI was calculated by expression suggested by reference⁶. The equations Eq. 5.1.1 and Eq. 5.1.2 allow us to obtain a minimum value of the thickness s_{in} (Figure 33) that reaches the bending stiffness target but by the equations Eq. 5.1.3 and Eq. 5.1.4 it is possible to get minimum value of the thickness s_{in} (3 mm) to avoid the buckling phenomenon (Figure 34). Then a FEM analysis was performed to verify the theoretical data, at this stage, it was possible to confirm the thickness s_{in} , the number N of carbon fiber plies inside the laminate, and the fabric orientations.

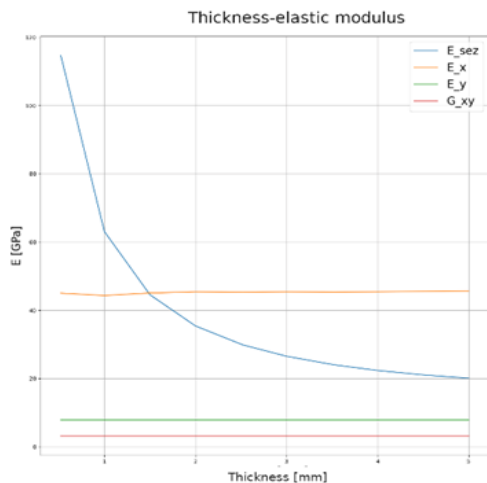


Figure 33 - Results of the elastic modulus obtained with Eq. 5.1.1 and Eq. 5.1.2

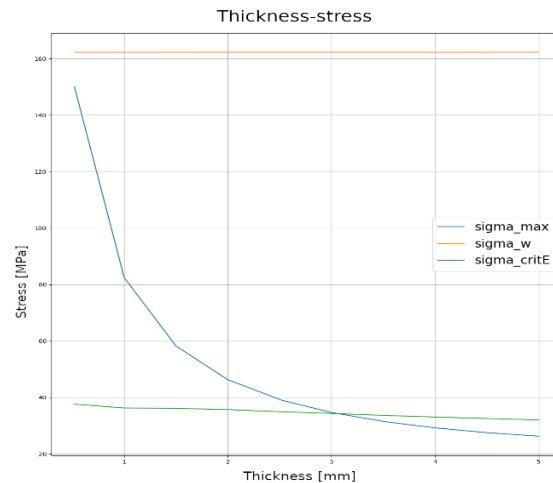


Figure 34 - Results of the elastic modulus obtained with Eq. 5.1.3 and Eq. 5.1.4

³ Robin Olsson. Composite Mechanics and laminate theory. Department of Aeronautics, Imperial College, 2006.

⁴ M. Palantera. ESAComp3.2 Theoretical Background of ESAComp Analyses, 1998.

⁵ T.H.G. Megson. Aircraft Structures for engineering students. Elsevier, 2007.

⁶ K.A. Wang E.E. Gdoutos I.M. Daniel e J.L. Abot. "Nonlinear Behavior of Composite Sandwich Beams in Three-point Bending". In: Springer 41, 2001.

The fibers of the plies were arranged along the axis of the beams. To study the cutting flow inside the wing skin due to the stabilizer torque, the theory of idealized closed section structures was used⁵. The wing was considered to be composed by three cells so we can study the wing torsion stress using:

$$M_T = \sum_{r=1}^3 2A_r q_r, \quad \frac{d\theta}{dz} = \frac{1}{2} \oint \frac{q_r ds}{A_r G_r S} \quad \text{Eq. 5.1.5}$$

from which we obtain a system of four equations by four unknowns where q_r by $r = 1,2,3$ are of interest. The wing's skin is made of composite material with a sandwich configuration, inside the sandwich there is a polyurethane (Airex) panel with a thickness of 1.2 mm. Since the carbon fiber laminates thickness are much lower than the polyurethane layer, it was possible to use thickness “s” as a known term in the equation Eq. 5.1.5 and obtain cutting stress which results lower than 5 MPa. By this time, it was decided the carbon fiber plies orientation and the number of plies. We ended up using a +45° biaxial 50 g/m² carbon fabric lamina on each side of 1.2 mm thickness Airex polyurethane layer to make up the sandwich panel. The rear spars are made of the same sandwich panel that was used for the wing skin but the UD fabrics are substituted with plain weave. Once the wing engineering constants were defined

$$E_x = \frac{1}{a_{11}^*}, \quad E_y = \frac{1}{a_{22}^*}, \quad G_{xy} = \frac{1}{a_{66}^*}, \quad s_{in}, \quad s, \quad \sigma_{max}, \quad \tau_{max}$$

Now it was possible to perform a FEM analysis of the wing and the results are shown in *Figure 35*.

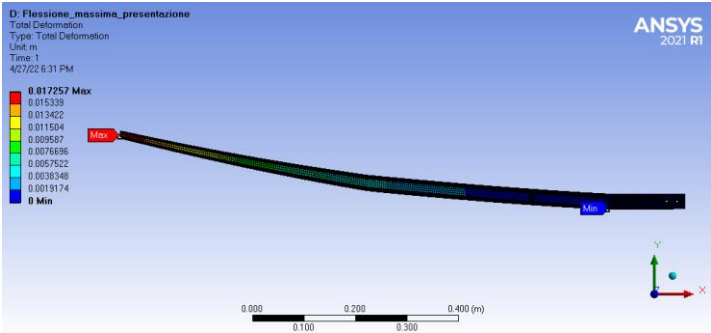


Figure 35 - Maximum total deformation from FEM analysis (left wing)



Figure 36 - Wing structural test



Figure 37 - Wing construction before closing the wing skins



Figure 38 - Molds used to produce the composite components for the wing skin



Figure 39 - Main spars molds

Figure 36 shows the structural test of the entire wing made in our laboratory. The entire wing structure was produced by using moulds. Figure 38 shows the wing skin moulds made with a CNC router, while Figure 39 shows the main spar moulds.

The aerodynamic design of the winglets have been described in Paragraph 4.3. They are made of a sandwich structure similar to the wing structure, with a carbon skin and Airex core. They were made by hand lamination into 2 moulds (pressure and suction side) produced with 3D printing technology (Figure 40). The winglets are inserted and fixed at the end of the wings thanks to two carbon rods.

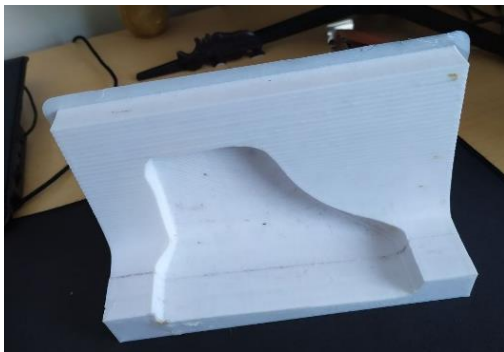


Figure 40 - Mould of winglets produced by 3D printing technology

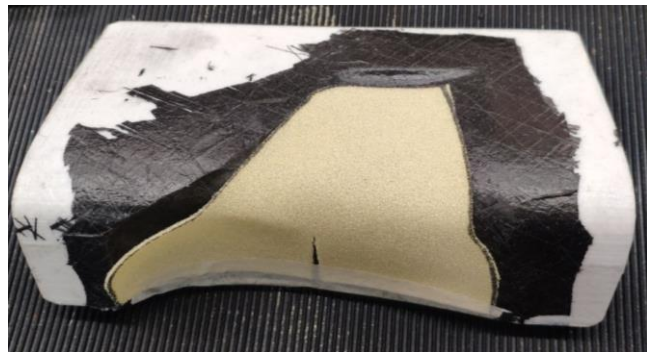


Figure 41 - Laminating sandwich structure on the winglet mould

6.2 FUSELAGE DESIGN

The fuselage is the central component of the plane and thus must interface with most of the other parts of the aircraft. For this reason, the design needs to be carried on along with the development of the other subsystem leading to an iterative and complex procedure. The main purposes that the fuselage must fulfill are:

- to contain the payload and the electronic system;
- to allow an easy load and unload of the payload;
- to position the other components in the right spots as to have the CG in the desired longitudinal position;
- to connect all the other subsystems of the plane (wing, undercarriage, motor);
- to guarantee that loads can be transmitted between wing, motor, and undercarriage.

An initial design of the general shape has been developed in collaboration with the flight mechanics division and aerodynamic division. The first choice regarding the building process concerned the type of material to be used for the construction since this decision would have influenced all the subsequent designs. Two main options were considered: the first one was a composite monocoque, while the other was a fuselage with an internal structural frame and external light and aerodynamic cover. To choose between the two, a comparison was made in terms of weight, previous experience, and construction procedures needed. The weight was roughly estimated by sketching a CAD model of both options, and the results were in favor of the monocoque. Thanks to the experience gained with Marcoplano, our plane for the ACC 2019, the team had sufficient knowledge and tools to build composite components so, in the end, the choice was made easily.

In the end, we decided on a monocoque made of a composite sandwich. The core is a 2 mm Airex (PVC foam) panel, and the fiber reinforcement is one ply of spread tow carbon fiber fabric (1 ply of CF - 2 mm of Airex - 1 ply of CF). Additional patches of aramidic fiber were placed where the undercarriages are fixed to the fuselage to dissipate energy coming from hard landings. Other stripes of monodirectional carbon fiber were added in strategic places to stiffen the fuselage. The layup was initially chosen based on the experience of the team and then validated with a FEM analysis and various tests in which we compared different amounts of plies in terms of weight and stiffness

obtained. After the design was completed it was time to create the molds and practice the use of Airex which was new for the team. In the beginning, the aim was to build the two symmetrical molds from scratch in the lab of the team but, due to the lack of a CNC milling machine and a 3D printer, we ended up needing to build the molds from a master. Way too much time was spent on building the master from scratch (Figure 42) but fortunately, the team was able to get machined molds from a new sponsor. The handmade molds were used for tests while the machined ones for the prototype and the official plane.

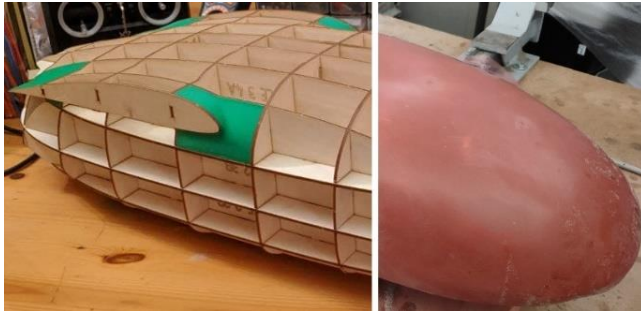


Figure 42 - Handmade master during and after construction



Figure 43 - Inside of the fuselage of the prototype drone

Due to a lack of experience in using Airex, we found it necessary to test different types of building techniques. In the beginning, the prototype was built by hand with wet layup and vacuum bagging, but the fuselage resulted to be too heavy. The problem was the excess of resin in the fibers and the additional resin necessary to glue down the core. Moreover, we found it necessary to laminate the plies and glue the Airex in three different steps resulting in a long process. Trying to reduce the weight of the sandwich, we conducted a series of different tests to find the best method that could also allow for a quicker build. In the end, the best solution was to use the RTM method. In this way the result is more predictable and lighter. Probably, with more tests and practice, the weight could be further decreased.

6.3 CARGO BAY

The payload is placed inside a box open on the upper side that can store up to ten bags. It is equipped with an elastic band to firmly hold down the water bags. The cargo box is positioned in the fuselage and can be locked in place by the use of magnets that provide a quick and strong hold. When the box is in position, one of the magnets has a pin that falls inside the hole of the opposite magnet, built similarly to a washer. In this way, the movement of the box is prevented mechanically. The fuselage can be opened from the front by rotating upward the nose which is held in place with other magnets when is closed. The hinge is made out of simple duct tape. The use of magnets and elastic bands make it possible to load and unload the payload in the shortest time possible. The box and its supports are made of a sandwich carbon fiber panel for minimum weight. This building method was used also for the battery holder and the GPS holder.

6.4 TAIL DESIGN

Considering the aerodynamic geometry, we decided to realize the surfaces of the tail with a sandwich panel structure, having an internal core of XPS (extruded polystyrene) that provides the shape of the airfoil on which is then laminated a carbon fiber composite and epoxy resin skin. In addition, a unidirectional carbon fiber reinforcement is laminated between the core and the skin at $c/4$ to provide flexural stiffness to the structure. The skin consists of a biaxial carbon fabric placed at

+45°, thus providing torsional stiffness to the structure. The connection between the tailplane and the boom was made using a carbon skin positioned at the c/4 to minimize the torque. The same approach was used for the construction of the central connector and the pitch fins.

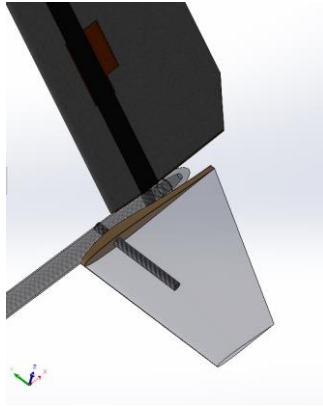


Figure 44 - Pitch fin structure



Figure 45 – Servo installation inside the tailplane

To allow the movement of the moving surfaces, a servo is inserted inside the XPS core. The case of the motor is fixed to the tailplane while the rotor is fixed to the carbon tube. In this way, it is possible to have a servo-control completely housed inside the surfaces (reducing aerodynamic impact) and with a motion transmission system with no mechanical backlash except for the one intrinsic to the servo-control.

At this point, a FEM analysis of the moving surfaces and the central connector has been carried out to understand the resistance and stiffness offered by the structure, as well as to identify the most critical points to be reinforced. To do that, it was necessary to characterize the elastic and breaking properties of the used materials. The data provided by manufacturers have been used and, where not present, have been integrated with data available in the literature. We carried out a linear elastic analysis that wants to be representative of a test carried out in the laboratory. In particular, it was intended to simulate the application of a load uniformly distributed on the extrados using sandbags. The applied load wants to represent the aerodynamic forces that act on the structure when the airfoil develops the maximum lift coefficient at maximum speed. In these conditions the lift developed by the tail assembly with a safety factor $n = 1.4$ results equal to:

$$L = n \frac{1}{2} \rho V^2 C_L S = 49.53 N \quad \text{with } V = 24 \text{ m/s } C_L = 0.91$$

Consequently, a distributed load equal to $W/S = (L/S)/\cos(40^\circ) = 585.69 \text{ Pa}$ was applied together with the force generated by the gravity acceleration acting on the mass of the structure. Using fixed constraints at the end of the booms and exploiting the symmetry of the structure, the following results are obtained:

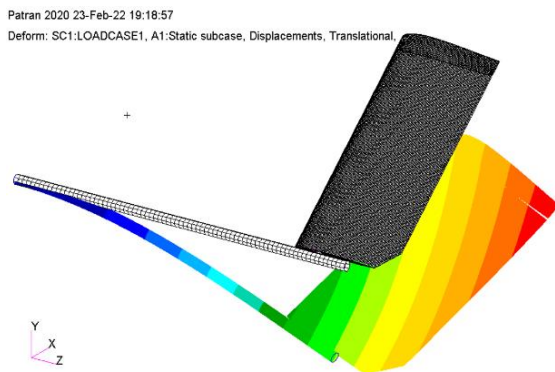


Figure 46 - Translational displacement

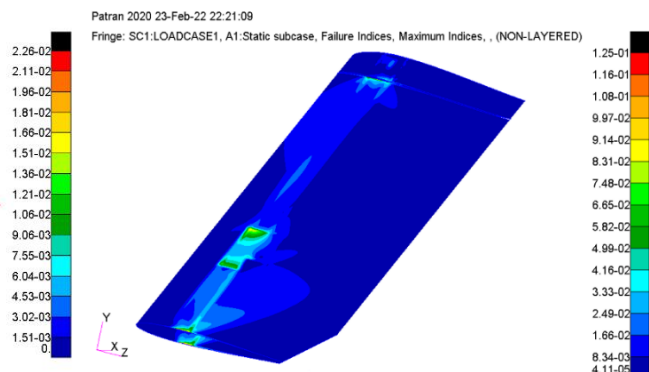


Figure 47 - Maximum failure indices

As a result of the load, the structure deforms downward and the booms tend to widen, with maximum absolute displacements on the order of 1.3 cm for the booms and 2.3 cm for the surfaces and the central connector. Observing for example the maximum failure indices (*Figure 47*) for the carbon skin of the mobile surfaces, we notice that the maximum values are of the order of 0.125, well below 1, therefore the structure results adequately resistant and rigid. Nevertheless, we can see how the most critical zone results just in correspondence with the servo control following the discontinuity in the XPS. This suggests that it is necessary to add further reinforcement fabrics in this zone. The results obtained from the FEM were then validated with laboratory tests, in particular, the vertical Δy displacement and horizontal Δx displacement values of the booms were compared, obtaining the following results:

	Δy	Δx
FEM	$1.36 \cdot 10^{-2} m$	$6.4 \cdot 10^{-3} m$
Laboratory	$2.10 \cdot 10^{-2} m (+54.4\%)$	$8.0 \cdot 10^{-3} m (+25.0\%)$

We can see that the results on the vertical displacement are not so in accordance with the FEM model. The main cause is due to the not perfect realization of the joint in the experimental setup (made with clamps). On the other hand, the displacement Δx shows a much better match.



Figure 48 - Test setup



Figure 49 - Loading the tailplane assembly



Figure 50 - Test with the car in motion

Further tests have been carried out to verify the correct operating of the kinematic mechanism inside the surface and to verify that it was able to provide the required torques in flight. A tail surface was installed inside a car (*Figure 50*) and exposed to the flow generated by the running car; it was decided to test the surface under the most severe conditions assumed in the static test, i.e. at the maximum cruising speed (measured with the car speedometer) and at an AoA close to the stall. To visually identify the stall of the airfoil, wool threads were installed on a portion of the surface as visible in the photos. The tests were successfully completed and qualified the structure for flight.

6.5 LANDING GEAR DESIGN

Due to project choices inherent to different subsystems, it was decided to use a tricycle configuration. This decision was almost obligatory for two main reasons: first of all the tailplane is characterized by a peculiar shape that does not let room for any back wheel as, for example, in the taildragger configuration; the second reason is the pusher configuration of the propeller, which requires keeping a fixed clearance from the terrain to properly work. Both gear legs are made with a structure of sandwich composite, with layers of mainly unidirectional carbon fiber for flexural strength coupled with Airex as the core material. The base idea is to realize flexible structures, which can easily sustain the impact and dampen the forces during the landing. After the preparation of the molds, the manufacturing finally started, which inevitably led to unsuccessful results and the arising of many problems due to our inexperience (past landing gear was simply made of aluminum alloy):

- Design errors, mainly on the nose gear
- Wrong choice of the carbon fabrics
- Mistakes during the lamination process
- Low aerodynamical efficiency, especially on the nose gear
- Structural faults especially for the nose gear

These first attempts of lamination were done with the vacuum bag + infusion technique, but due to a combination of the high number of layers, the shape of the gears, and again, our inexperience, it was obvious that this method did not allow for a uniform flow of resin. The final decision was to opt for the vacuum bag but to apply the resin manually on every layer of carbon fiber. Regarding structural faults, the nose gear was the main source of problems. The original design was expected to be that of a sandwich panel with a relatively thin but large rectangular section. After the manufacturing, it was tested to the nominal maximum load and it was immediately clear that it could not properly sustain the vertical load and it was particularly sensible to torsion. Therefore the section width was increased, along with the number of layers of carbon fiber. Also instead of only unidirectional fabrics, it was decided to mainly use ± 90 fabrics instead and reinforcements were added both to the front and rear zone, which also helped decrease the aerodynamic drag produced by the nose gear. The main gear showed fewer problems: it only required an optimization of the positioning of the carbon fiber layers and the addition of two reinforcements near the curvature, which can be seen in the image below.

After the introduction of these changes, we conducted a FEM analysis, thanks to which we were able to verify the reinforcement's effectiveness. Both gears were constructed and tested again, this time they were required to withstand a static load up to 3x the nominal maximum load of 6 kg. The aim was to simulate the dynamic load during landing. The results showed how essential the changes mentioned before are since both the nose and main gear managed to sustain 20 kg of load with ease. Eventually, real tests in the airfield were done, showing that structurally speaking there are no problems, apart from an excessive stiffness that required a better optimization. To do this we worked on the previously made FEM analysis and we tried to optimize both the number of layers and the size of the reinforcements, also managing to achieve a weight reduction.

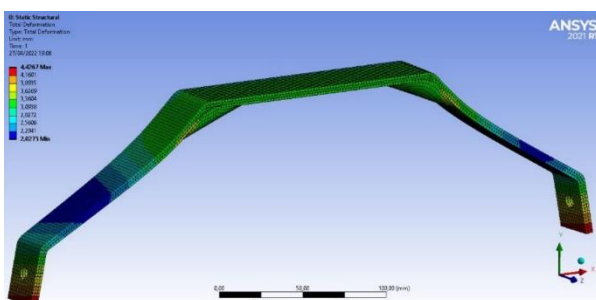


Figure 51 – Main gear, total deformation

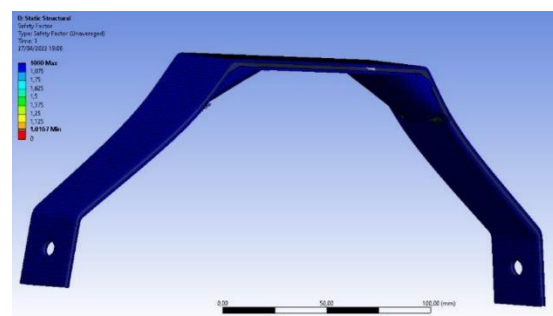


Figure 52 – Main gear, safety factor

The main gear reinforcements were reduced in size and also the number of layers was reduced. The results were promising, they were compatible with the experimental test and the project requirements.

The nose gear also underwent similar changes as the number of layers was decreased along with the size of the reinforcement. Furthermore, the manufacturing process of the latter was significantly reduced since it was decided to use a special foam that will expand on specific molds realized with a 3D printer. This means it is possible to obtain the final shape with fewer passages, which means less time, errors, and more efficiency. The foam core was then wrapped with carbon fiber, reducing the number of layers and resin utilized.

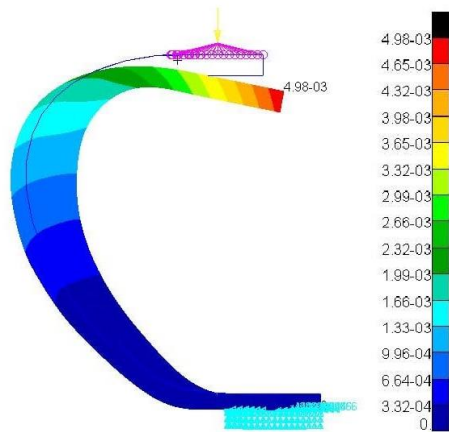


Figure 53 – Nose gear, translation displacements

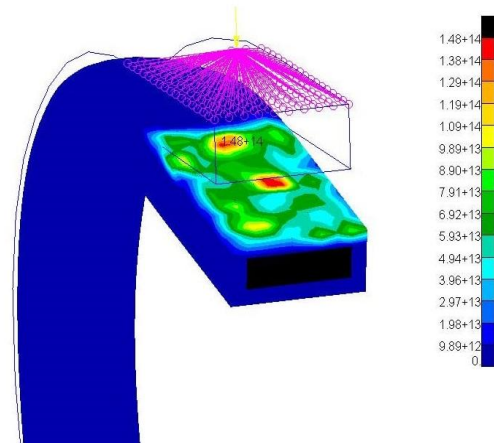


Figure 54 – Nose gear, max strenght ratios

Both gears are fixed to the fuselage with 2 bolts with self-locking nuts (to avoid loosening of the connection due to vibrations produced by the motor), so the bolts can be disassembled to remove the gears and fit them into the transportation box. We decided to design the wheels to be narrower than common wheels used in similar applications, mainly to reduce the aerodynamic drag produced by that kind of wide wheel. The diameter was chosen to better satisfy the requirements for propeller and tailplane clearance from the ground in the steeper configuration of the aircraft. Two different production processes for the wheels were utilized: the first batch of wheels were made in PLA using a 3D printer, the second with birch wood instead. Both kinds of wheels were designed to make possible the implementation of bearings for reducing mechanical friction.

7 ELECTRONIC SYSTEMS

The configuration of the electronic system of the aircraft is determined by the regulation, so the aspect on which the electronics division has mainly focused is the choice of components. Regarding the main battery, we used 3s LiPo with high discharge rate in order to obtain the maximum possible power at takeoff. We are evaluating what is the best battery capacity to use and we need to find a compromise between weight and final voltage (higher capacity means more weight but also more power in the final phase of the flight); however, we assume that we will use a capacity between 3000mAh - 4500mAh. The choice of the servos has been made taking into account the following aspects:

- maximum torque developed at the power supply voltage (equal to the battery voltage of the receiver, which is a 2s LiPo having a nominal voltage of 7.4V);
- dimensions: in particular for the tailplane, the need to install the servos inside a surface with a maximum thickness of 1.4 mm makes it necessary to find sufficiently thin servos;
- speed and precision: from the experience of past aircrafts, it has been realized the importance of having a precise and fast servo-control in order to guarantee the most precise piloting;
- weight: considering a total number of 6 servos, the difference in weight can be significant.

Regarding the propeller, the regulation allows the choice between 3 different models. In order to identify the best model, it was decided to build a test bench (Figure 55), controlled by Arduino, able to measure the static thrust and the counter-torque generated through the use of 3 load cells. The Arduino interfaces with Matlab and allows obtaining real-time data measured at the test bench. The test bench has been recently completed, and so far has been used to verify that the Aeronaut CAMcarbon 10x6 propeller develops similar performance in pulling and pushing configuration. It was

also found that with this propeller we can reach a peak current of 23A, this data was useful to choose the correct ESC.

In order to study the flight performance of the aircraft, the project is dealing with the installation of a control unit on board of the aircraft that should be able to receive and eventually transmit real-time data from sensors such as Pitot tube, GPS, accelerometers, and gyroscopes. This data will be used for multiple purposes including:

- calculating the score for each flight based on ACC2022 regulations;
- implementing a warning system on the radio that alerts the pilot if he gets too close to stall speed;
- measure flight path angle of climb and airspeed in cruise condition in order to compare the data with the project requirements.

This control unit has been already installed inside Marcoplano (ACC2019 competition aircraft), in the next months it will be installed inside the prototype object of this document.

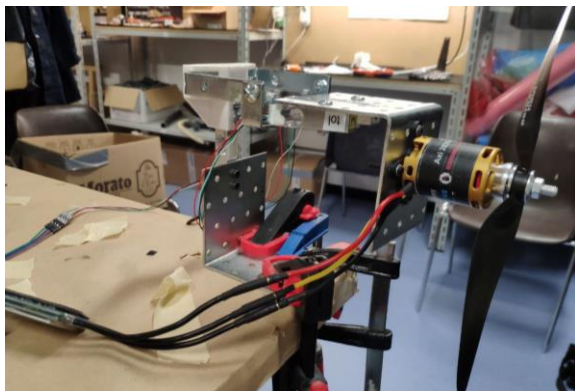


Figure 55 – Propeller test bench



Figure 56 - Pitot tube mounted on Marcoplano (ACC2019)

8 OUTLOOK

In the coming months, the project will focus on the production and testing of the definitive aircraft that going to fly to the ACC2022 competition. The final aircraft is going to be a structural optimization of the prototype, meaning that we are going to make lighter the structures where they proved to be more rigid and resistant than expected with consequent benefit in carrying a greater payload. In the meantime, flight tests with the prototype will continue and we will exploit the data we get from the telemetry to validate the mathematical models developed and the flight behavior of the aircraft.

In addition to this, we are developing a flight simulator in a Matlab - Simulink environment that can be interfaced with the radio control, which will have multiple purposes: allowing us to identify the optimal characteristics in terms of stability and controllability for future aircraft, provide a useful environment for the pilot to become familiar with the aircraft and train on the flight path.

Furthermore, a traction machine designed by us is under construction, in this way we will be able to test the composite material specimens. Thanks to the traction machine we will be able to obtain the force-displacement curves of the carbon specimens built internally for the project.

The propeller test bench we have developed will be used in the coming months to carry out a series of studies that includes: comparing the performance of the 3 propellers allowed by the regulation to identify the best performing one, testing the performance of the ogive to understand if its additional mass justifies its advantages, understanding the degradation of performance associated with the

increase in temperature of the various electronic components and therefore the effectiveness of interventions such as air inlets or refrigerant sprays.

We also intend to carry out stall tests of the aircraft and study it after each flight thanks to the videos recorded by a video camera installed in the upper area of the fuselage. The video camera points towards the tip of the wing and records the movement of the woolen threads applied to the wing skin. Once the aircraft is at a safe altitude, the stall is induced and by analyzing the behavior of the wool threads it is possible to understand where the stall begins to develop and how it spreads to the rest of the wing. In addition, there will be a test for the analysis of structural vibrations to which the wing is subjected in flight using a stereocamera. Through specific algorithms⁷ ⁸ it is possible to analyze the videos recorded to extrapolate the positions of the objects with respect to the device. Knowing the positions of the objects instant by instant it is then possible to analyze their speed and acceleration with respect to the stereocamera⁹.



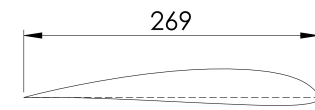
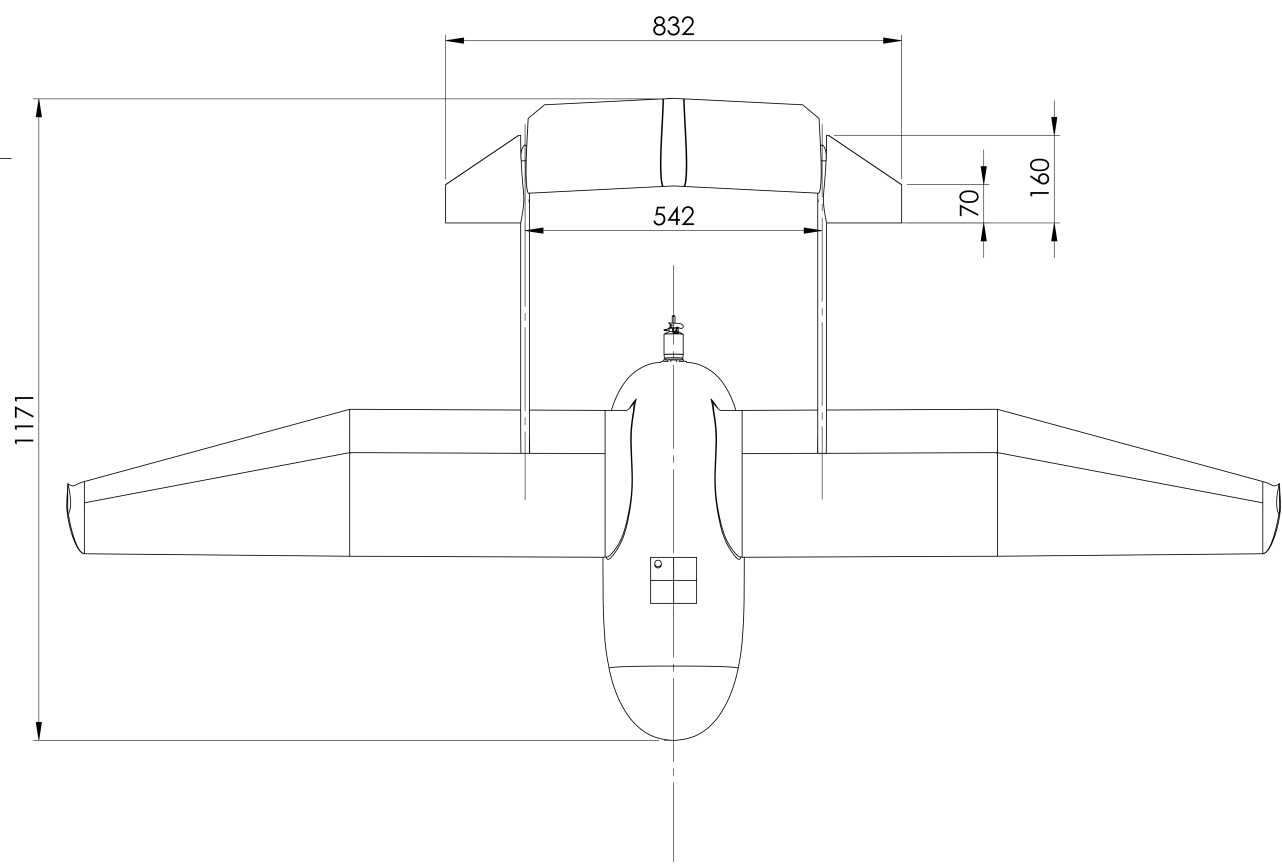
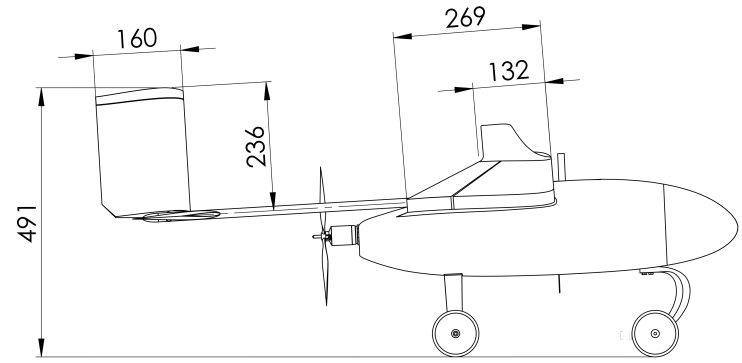
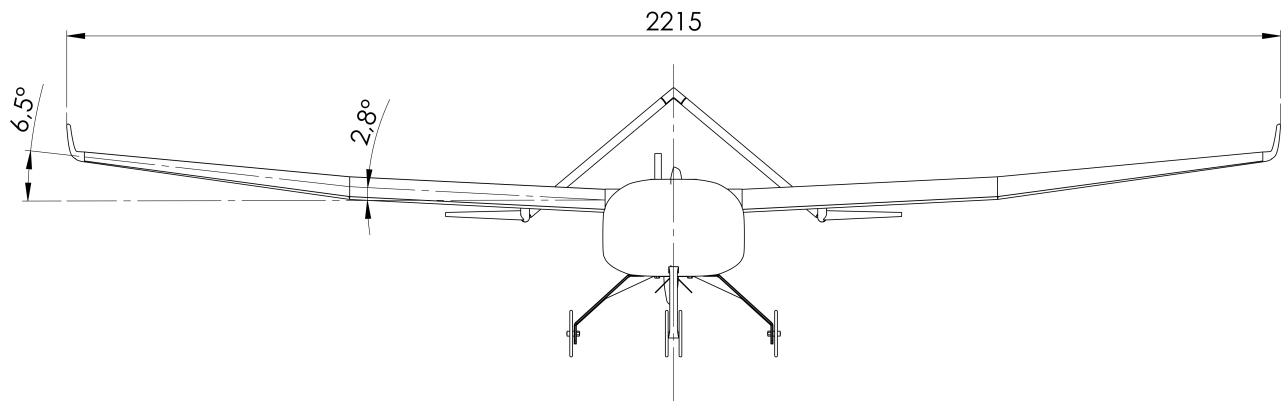
⁷ Peter Corke. Robotics, Vision and Control Fundamental Algorithms in MATLAB. Springer, 2011.

⁸ OpenCV Camera Calibration and 3D Reconstruction

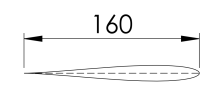
https://docs.opencv.org/4.5.5/d9/d0c/group__calib3d.html#ga7dfb72c9cf9780a347fbe3d1c47e5d5a

⁹ Yanda Shao, Ling Li, Jun Li, Senjian An, Hong Hao. Computer vision based target-free 3D vibration displacement measurement of structures. Elsevier, 2021

9 DRAWINGS



ROOT WING AIRFOIL
SCALE 1:5



TAIL AIRFOIL
SCALE 1:5

Wing airfoil	Opt06v3
Tail airfoil	Joukowski 0009
Pitch fin airfoil	Joukowski 0009
Wing surface	0,445m ²
Tailplane surface	0,110m ²
Tailplane dihedral angle	-40°

NAME: 3-View Drawing

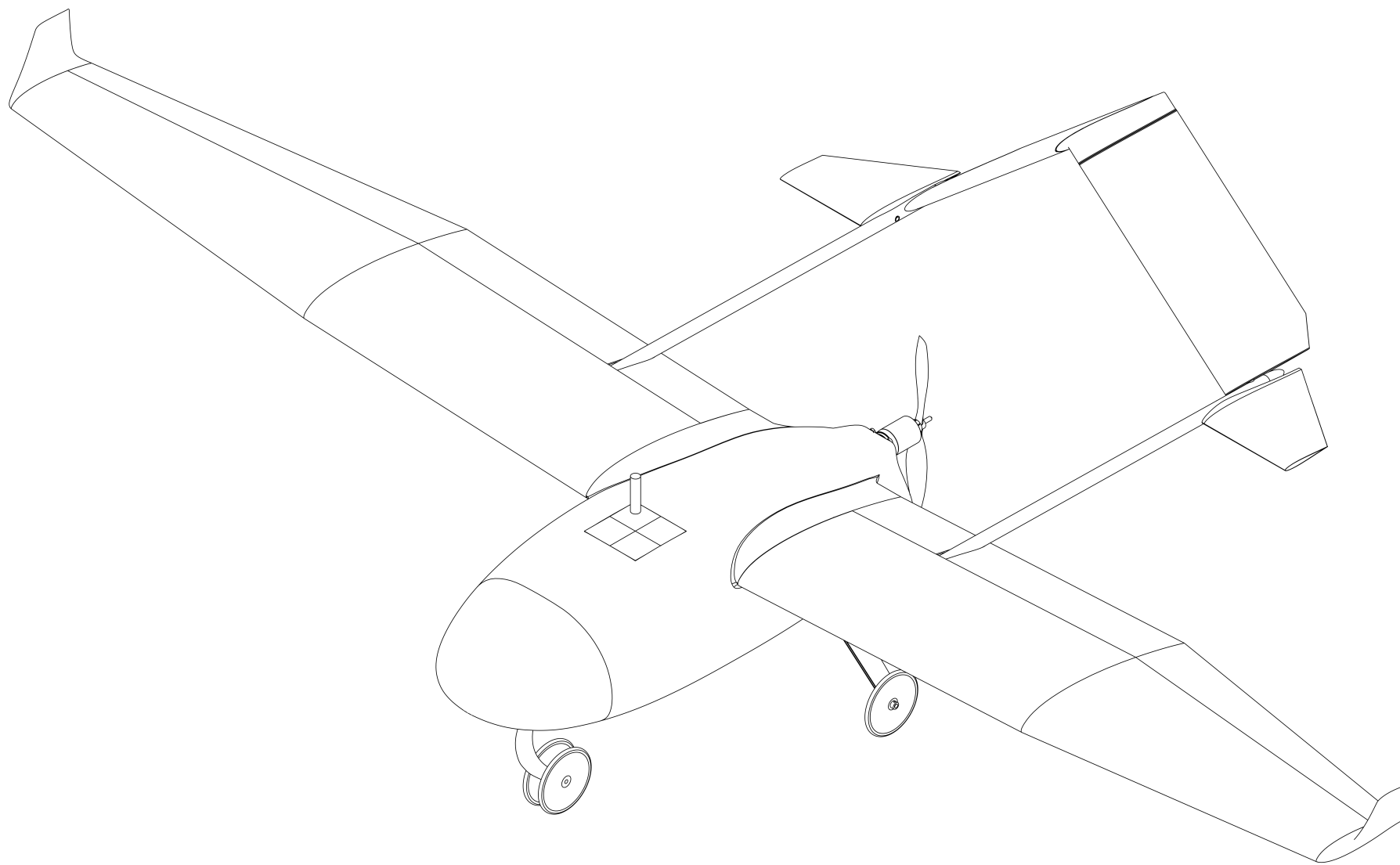


UNIVERSITA
DEGLI STUDI
DI PADOVA

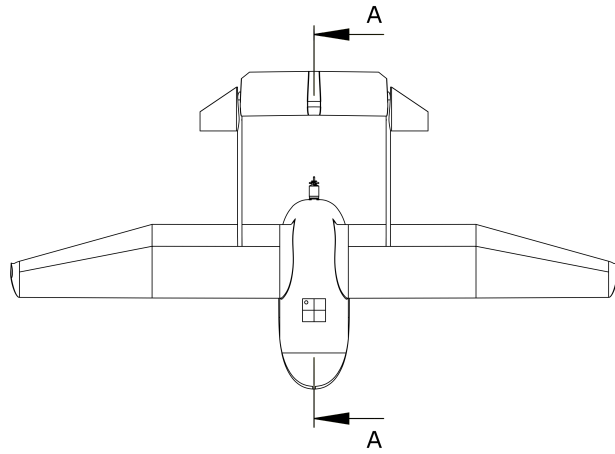


TEAM'S
NUMBER:
14

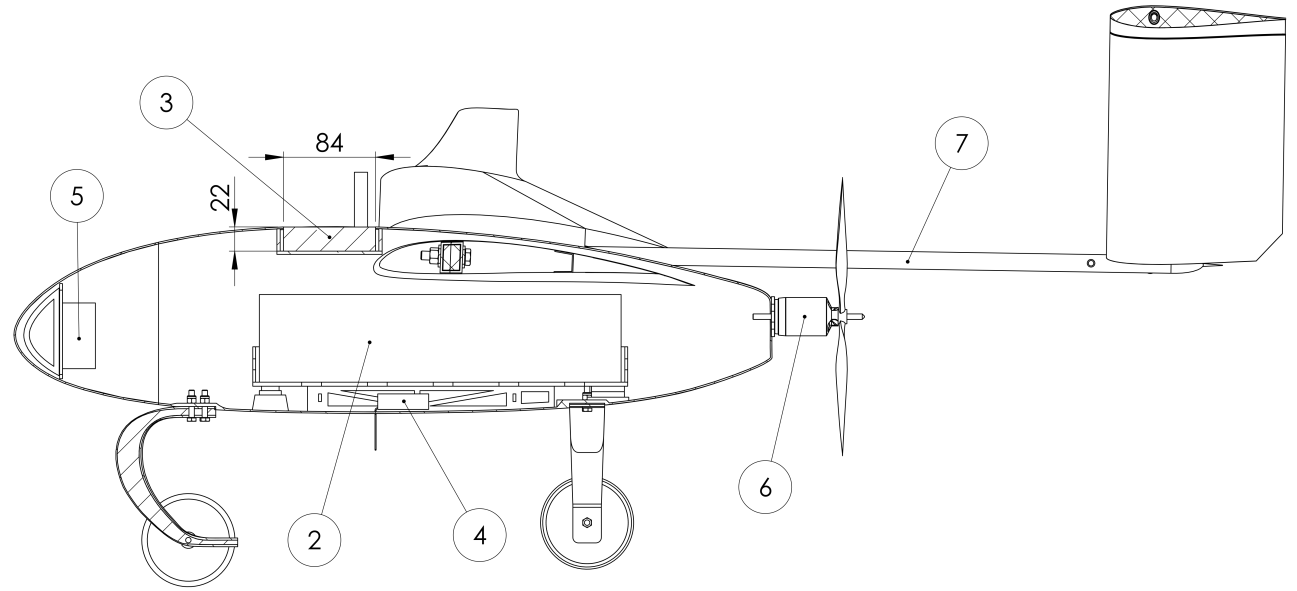
AUTHOR: Lift UP Team		A3
DATE: 30/04/2022		



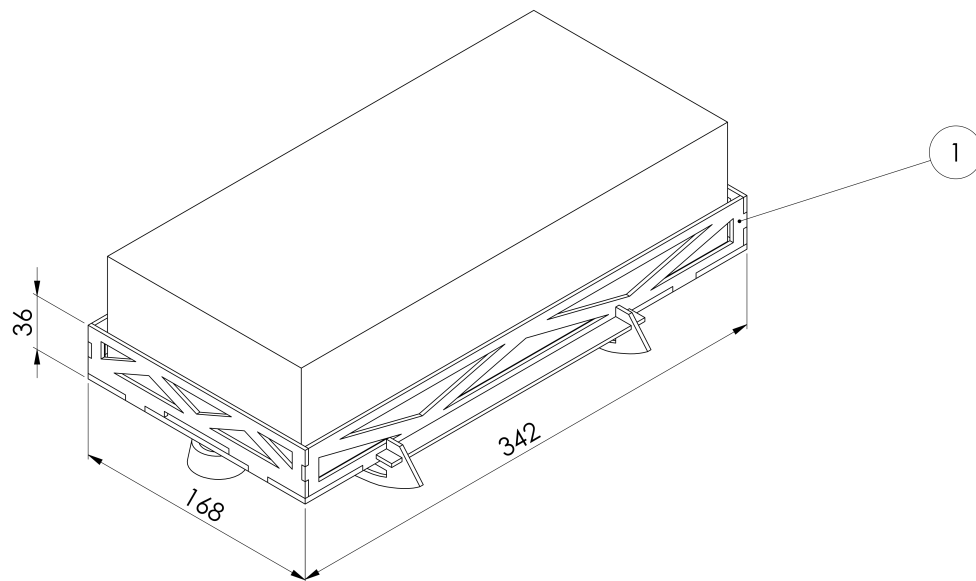
NAME:		Isometric view	
	UNIVERSITÀ DEGLI STUDI DI PADOVA		TEAM'S NUMBER: 14
AUTHOR: Lift Up Team			A3
DATE: 30/04/2022	SCALE: 1:5		



SCALE 1 : 20



SECTION A-A
1 : 5

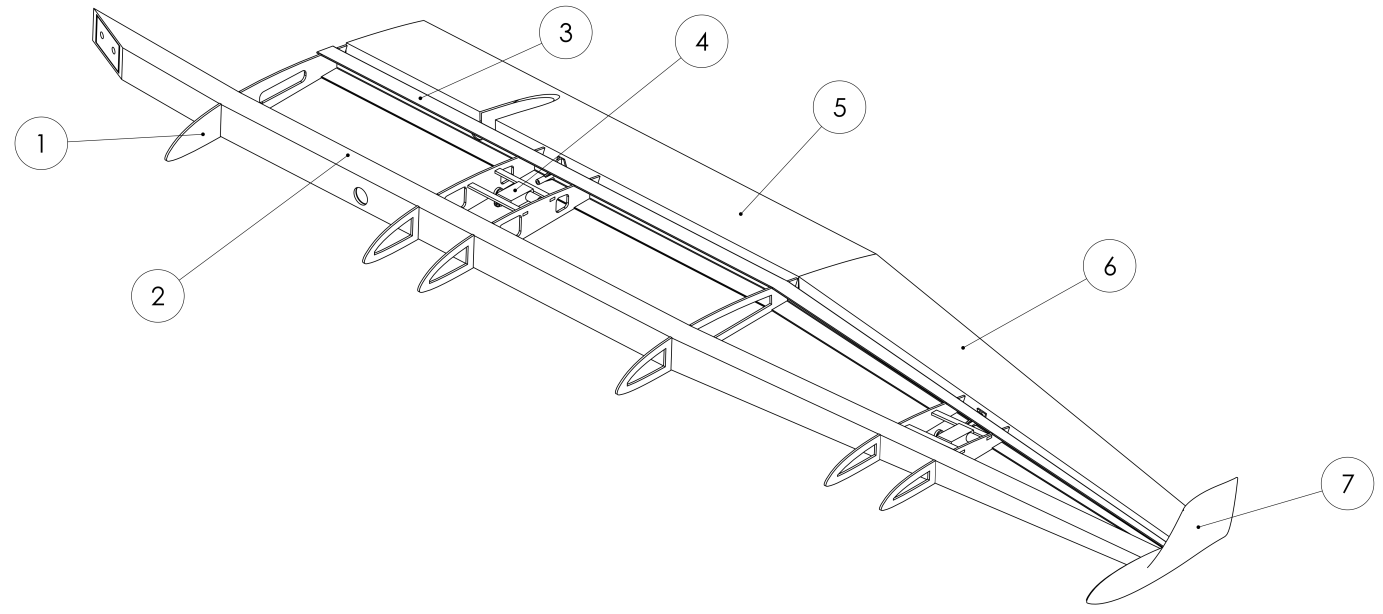
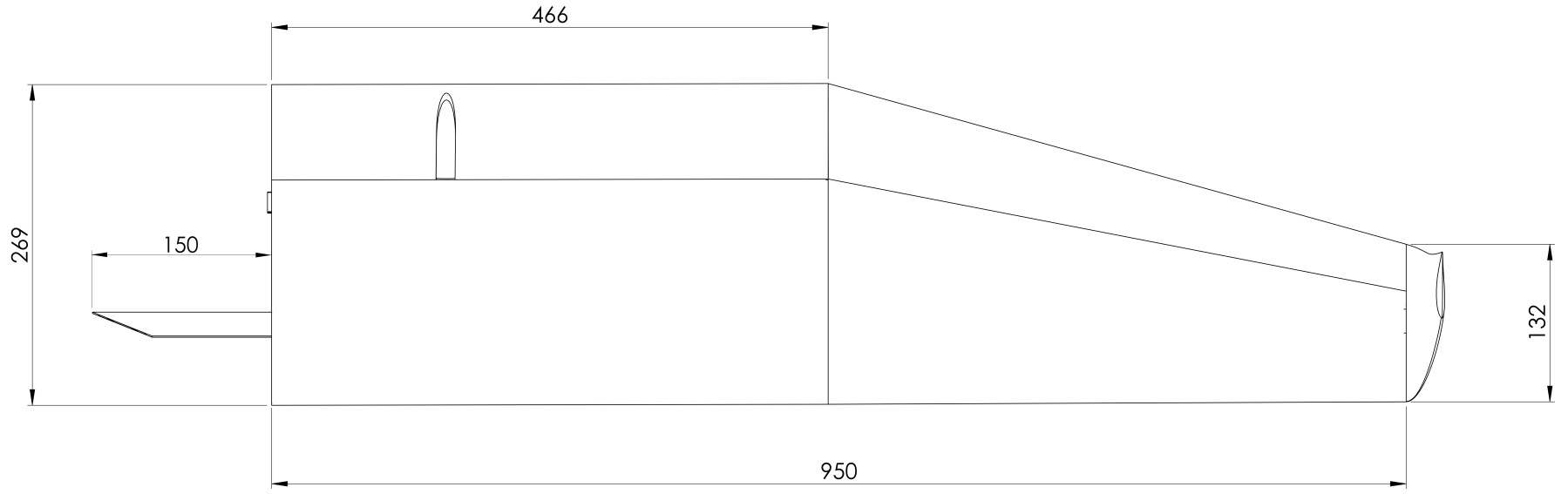


SCALE 1 : 3

NUMBER	NAME
1	Cargobox
2	Payload
3	GPS equipment
4	RC Receiver
5	Battery
6	Motor + propeller *
7	Boom

* The propeller is fixed to the motor shaft with a airscrew nut

NAME: Cargobox - receiver - GPS location	
 UNIVERSITÀ DEGLI STUDI DI PADOVA	LIFT UP
AUTHOR: Lift UP Team	TEAM'S NUMBER: 14
DATE: 30/04/2022	



NUMBER	NAME
1	Rib
2	Main spar
3	Second spar
4	Servomotor
5	Flap
6	Aileron
7	Winglet

NAME: Wing View



TEAM'S NUMBER: 14

AUTHOR: Lift Up Team

DATE: 25/04/2022

SCALE: 1:4



A3